Atmos. Chem. Phys. Discuss., https://doi.org/10.5194/acp-2019-206
Manuscript under review for journal Atmos. Chem. Phys.
Discussion started: 16 April 2019

Atmospheric Chemistry and Physics Discussions

Evidence from IASI of a speeding up in stratospheric O_3 recovery in the Southern Hemisphere contrasting with a decline in the Northern Hemisphere

Catherine Wespes[1], Daniel Hurtmans[1], Simon Chabrillat[2], Gaétane Ronsmans[1], Cathy Clerbaux[3,1] and Pierre-François Coheur[1]

[1]Université Libre de Bruxelles (ULB), Faculté des Sciences, Chimie Quantique et Photophysique, Bruxelles, Belgique
[2] Belgian Institute for Space Aeronomy, Brussels, Belgium
[3] LATMOS/IPSL, Sorbonne Université, UVSQ, CNRS, Paris, France

Abstract

In this paper, we present the global fingerprint of recent changes in the mid-upper stratospheric (MUSt; >25hPa) ozone (O_3) in comparison with the lower stratospheric (LSt, 150-25 hPa) O_3 derived from the first 10 years of the IASI/Metop-A satellite measurements (January 2008 – December 2017). The IASI instrument provides vertically-resolved O_3 profiles with very high spatial and temporal (twice daily) samplings, allowing to monitor O_3 changes in these two regions of the stratosphere. By applying multivariate regression models with adapted geophysical proxies on daily mean O_3 time series, we discriminate anthropogenic trends from various modes of natural variability, such as the El Niño/Southern Oscillation – ENSO. The representativeness of the O_3 response to its natural drivers is first examined. One important finding relies on a pronounced contrast between a positive LSt O_3 response to ENSO in the extra-tropics and a negative one in the tropics, with a delay of 3 months, which supports a stratospheric pathway for the ENSO influence on lower stratospheric and tropospheric O_3. In terms of trends, we find an unequivocal O_3 recovery from the available period of measurements in winter/spring at mid-high latitudes for the two stratospheric layers sounded by IASI (>~35°N/S in the MUSt and >~45°S in the LSt) as well as in the total columns at southern latitudes (>~45°S) where the increase reaches its maximum. These results confirm the effectiveness of the Montreal protocol and its amendments, and represent the first detection of a significant recovery of O_3 concurrently in the lower, in the mid-upper stratosphere and in the total column from one single satellite dataset. A significant decline in O_3 at northern mid-latitudes in the LSt is also detected, especially in winter/spring of the northern hemisphere. Given counteracting trends in LSt and MUSt at these latitudes, the decline is not categorical in total O_3. When freezing the regression coefficients determined for each natural driver over the whole IASI period but adjusting a trend, we calculate a significant speeding up in the O_3 response to the decline of O_3 depleting substances (ODS) in the total column, in the LSt and, in a lesser extent, in the MUSt, at high southern latitudes over the year. A significant acceleration of the O_3 decline at northern mid-latitudes in the LSt and in the total column is also highlighted over the last years. That, specifically, needs urgent investigation for identifying its exact origin and apprehending its impact on climate change.

Atmos. Chem. Phys. Discuss., https://doi.org/10.5194/acp-2019-206
Manuscript under review for journal Atmos. Chem. Phys.
Discussion started: 16 April 2019

Atmospheric Chemistry and Physics Discussions

1 Introduction

Ozone is a key radiatively active gas of the Earth atmosphere, in both the troposphere and the stratosphere. While in the troposphere, O_3 acts as a strong pollutant and an important greenhouse gas, in the stratosphere, and more particularly in the middle-low stratosphere, it forms a protective layer for life on Earth against harmful solar radiation. In the 1980s, the scientific community motivated decision-makers for regulating the use of CFCs, after the unexpected discovery of the Antarctic ozone hole (Chubachi, 1984; Farman et al., 1985) induced by continued use of chlorofluorocarbons (CFC's; Molina and Rowland, 1974; Crutzen,1974); These latter are at the origin of the massive destruction of O_3 following heterogeneous reactions on the surface of polar stratospheric clouds (Solomon, 1999). The world's nations reacted to that human-caused worldwide problem by ratifying the International Vienna Convention for the Protection of the Ozone Layer in 1985 and the Montreal Protocol in 1987 with its later amendments, which forced the progressive banning of these ozone depleting substances (ODS) in industrial applications by early 1990s with a total phase-out of the most harmful CFCs by the year 2000.

Ozone is very sensitive to changes in (photo-)chemistry, therefore a recovery from O_3 depletion is expected in response to the Montreal Protocol and its amendments, but with a delayed period due to the long residence time of halocarbons in the atmosphere (Hofmann et al., 1997; Dhomse el al., 2006; WMO, 2007; 2011). The decline in CFCs was only initiated about 10 years after their phasing out (Anderson et al., 2000; Newman et al., 2006; Solomon et al., 2006 ; Mäder et al., 2010; WMO, 2011; 2014). The early signs of ozone response to that decline were confirmed in several studies that reported first a slowdown in stratospheric ozone depletion (e.g. Newchurch et al., 2003; Yang et al., 2008), followed by a leveling off of upper stratospheric (e.g. WMO, 2007) and total O_3 (e.g. WMO, 2011; Shepherd et al., 2014) depletion since the 2000's. A significant onset of recovery was identified later for upper stratospheric O_3 (e.g. WMO, 2014; 2018; Harris et al., 2015). Only a few studies have shown evidence for increasing total column O_3 in polar region during springtime (e.g. Salby et al., 2011; Kuttippurath et al., 2013; Shepherd et al., 2014; Solomon et al., 2016). No reliable estimates of long-term trend in total O_3 columns (TOC) at global scale have been reported yet, likely because of counteracting trends in the different vertical atmospheric layers. Ball et al. (2018) have found that a continuing O_3 decline prevails in the low stratosphere since 1998, leading to a slower increase in total O_3 than expected from the effective equivalent stratospheric chlorine (EESC) decrease. However, the reported decline is not reproduced by the state-of-the-art models and its exact reasons are still unknown (Ball et al., 2018). Galytska et al. (2019) recently suggested that the decline is dynamically controlled by variations in the tropical upwelling.

Although recent papers based on observational datasets and statistical approaches agree that we currently progress towards an emergence into ozone recovery (e.g. Pawson et al., 2014; Harris et al., 2015; Steinbrecht et al., 2017; Sofieva et al., 2017; Ball et al., 2018; Weber et al., 2018), trend magnitude and trend significance over the whole stratosphere substantially differ from one study to another and, consequently, they are still subject to controversy (Keeble et al., 2018). A clear identification of the onset of O_3 recovery is very sensitive due to concurrent sources of O_3 fluctuations (e.g. Reinsel et al., 2005; WMO, 2007, 2011). They include: changes in solar ultraviolet irradiance, in atmospheric circulation patterns such as the quasi-biennial oscillation (QBO; Baldwin et al., 2001) and the El Niño–Southern Oscillation (ENSO; e.g. Randel et al., 2009), in temperature, in ODS emissions and volcanic eruptions (e.g. Mt Pinatubo in 1991 and Calbuco in 2015) with their feedbacks on stratospheric temperature and dynamics (e.g. Jonsson et al., 2004). Furthermore, the differences in vertical/spatial resolution and in retrieval methodologies (inducing biases), possible instrumental degradations (inducing drifts), and use of merged datasets into composites, likely explain part of the trend divergence between various studies. Merging may be performed on deseasonalized anomalies, which offers the advantage of removing instrumental biases between the individual data records (Sofieva et al., 2017) but large differences remain in anomaly values between the independent datasets, as well as large instrumental drifts and drift uncertainty estimates that prevent deriving statistically accurate trends (Harris et al., 2015; Hubert et al., 2016).

In this context, there is a pressing need for long-duration, high-density and homogenized O_3 profile dataset to assess significant O_3 changes in different parts of the stratosphere and their contributions to the total O_3.

In this paper, we exploit the high frequency (daily) and spatial coverage of the IASI satellite dataset over the first decade of the mission (January 2008 – December 2017) to determine global patterns of reliable trends in the stratospheric O_3 records, separately in the Mid-Upper Stratosphere (MUSt) and the Lower Stratosphere (LSt). This study is built on previous analysis of stratospheric O_3 trends from IASI, estimated on latitudinal averages over a shorter period (2008-2013) (Wespes et al., 2016). A multivariate linear regression (MLR) model (annual and seasonal formulations) that is similar to that previously used for tropospheric O_3 studies from IASI (Wespes et al., 2017; 2018), but adapted here for the stratosphere with appropriate drivers, is applied on gridded daily mean O_3 time series in the MUSt and the LSt. The MLR model is evaluated in terms of its performance and of its ability to capture the observed variability in Section 2, in terms of representativeness of O_3 drivers in Section 3 and in terms of adjusted trends in Section 4. The minimum numbers of years of IASI measurements that is required to indeed detect the adjusted trends from MLR in the two layers is also estimated in Section 4 that ends with an evaluation of the trends detectable in polar winter and spring and with an evaluation of a speeding up in the O_3 changes.

Atmos. Chem. Phys. Discuss., https://doi.org/10.5194/acp-2019-206
Manuscript under review for journal Atmos. Chem. Phys.
Discussion started: 16 April 2019

Atmospheric Chemistry and Physics Discussions

2 Dataset and methodology

2.1 IASI O_3 data

The Infrared Atmospheric Sounding Interferometer (IASI) is a nadir-viewing Fourier transform spectrometer designed to measure the thermal infrared emission of the Earth-atmosphere system between 645 and 2760 cm^{-1}. Measurements are taken from the polar sun-synchronous orbiting meteorological Metop series of satellites, every 50 km along the track of the satellite at nadir and over a swath of 2200 km across track. With more than 14 orbits a day and a field of view of four simultaneous footprints of 12 km at nadir, IASI provides global coverage of the Earth twice a day at about 09:30 AM and PM mean local solar time.

The Metop program consists of a series of three identical satellites successively launched to ensure homogenous measurements covering more than 15 years. Metop-A and –B have been successively launched in October 2006 and September 2012. The third and last satellite was launched in November 2018 onboard Metop-C. In addition to its exceptional spatio-temporal coverage, IASI also provides good spectral resolution and low radiometric noise, which allows the measurement of a series of gas-phase species and aerosols globally (e.g. Clerbaux et al., 2009; Hilton et al., 2012; Clarisse et al., 2018).

For this study, we use the O_3 profiles retrieved by the Fast Optimal Retrievals on Layers for IASI (FORLI-O_3; version 20151001) near-real time processing chain set up at ULB (See Hurtmans et al, 2012 for a description of the retrieval parameters and the FORLI performances). The FORLI algorithm relies on a fast radiative transfer and a retrieval methodology based on the Optimal Estimation Method (Rodgers, 2000) that requires a priori information (a priori profile and associated variance-covariance matrix). The FORLI-O_3 a priori consists of one single profile and one covariance matrix built from the global Logan/Labow/McPeters climatology (McPeters et al., 2007). The profiles are retrieved on a uniform 1 km vertical grid on 41 layers from surface to 40 km with an extra layer from 40 km to the top of the atmosphere considered at 60 km. Previous characterization of the FORLI-O_3 profiles (Wespes et al., 2016) have demonstrated a good vertical sensitivity of IASI to the O_3 measurement with up to 4 independent levels of information on the vertical profile in the troposphere and the stratosphere (MUSt; LSt; upper troposphere-lower stratosphere – UTLS – 300-150 hPa; middle-low troposphere − MLT – below 300 hPa). The two stratospheric layers that show distinctive patterns of O_3 distributions over the IASI decade (Fig.1a) are characterized by high sensitivity (DOFS > 0.85; Fig.1b) and low total retrieval errors (<5%; see Hurtmans et al., 2012; Wespes et al., 2016). The decorrelation between the MUSt and the LSt is further evidenced in Fig.1d that shows low correlation coefficients (< 0.4) between the mean absolute deseasonalized anomalies (as calculated in Wespes et al., 2017) in the two layers (Fig. 1c). Note that the highest correlation coefficients over the Antarctic (~0.4) are due to the smaller vertical sensitivity of the IASI measurements over cold surface (Clerbaux

et al., 2009). The latest validation exercises for the FORLI-O_3 product have demonstrated a high degree of precision with excellent consistency between the measurements taken from the two IASI instruments on Metop-A and -B, as well as a good degree of accuracy with biases lower than 20% in the stratospheric layers (Boynard et al., 2018; Keppens et al. 2017). Thanks to these good IASI-FORLI performances, large-scale dynamical modes of O_3 variations and long-term O_3 changes can be differentiated in the four retrieved layers (Wespes et al., 2016). The recent validations have, however, reported a drift in the MUSt FORLI-O_3 time series from comparison with O_3 sondes in the northern hemisphere (N.H.) (~3.53±3.09 DU.decade^{-1} on average over 2008–2016; Boynard et al., 2018) that was suggested to result from a pronounced discontinuity ("jump") rather than from a progressive change. Further comparisons with CTM simulations from the Belgian Assimilation System for Chemical ObsErvations (BASCOE; Huijnen et al., 2016; Chabrillat et al., 2018) confirm this jump that occurred on 15 September 2010 over all latitudes (see Fig. S1 of the supplementary materials). The discontinuity is suspected to result from updates in level-2 temperature data from Eumetsat that are used as inputs into FORLI (see Hurtmans et al., 2012). The apparent drift reported by Boynard et al. (2018) results from the jump and contrasts with a progressive "instrumental" drift. This is verified by the absence of drift in the O_3 time series after the jump (non-significant drift of -0.38±2.24 DU.decade^{-1} on average over October 2010 – May 2017; adapted from Boynard et al., 2018). This is in line with the excellent stability of the IASI Level-1 radiances over the full IASI period (Buffet et al., 2016). From the IASI-BASCOE comparisons, the amplitude of the jump has been estimated as lower than 2.0 DU in the 55°S–55°N latitude band and 4.0 DU in the 55°–90° latitude band of each hemisphere. The effect of the jump on the calculation of significant trends derived in Section 4 is found small enough to explain the trend, therefore, this estimated jump is not taken into account in the MLR. The jump values will be, however, considered in the discussion of the O_3 trends (Section 4).

Finally, the present study only uses the daytime measurements (defined with a solar zenith angle to the sun < 83°) from the IASI-A (aboard Metop-A) instrument that fully covers the first decade of the IASI mission. The daytime measurements are characterized by a higher vertical sensitivity (e.g. Clerbaux et al., 2009). Quality flags developed in previous IASI studies (e.g. Boynard et al., 2018) were applied a posteriori to exclude data with a poor spectral fit, with less reliability or with cloud contamination.

2.2 Multivariate regression model

In order to unambiguously discriminate anthropogenic trends in O_3 levels from the various modes of natural variability (illustrated globally in Fig.1c as deseasonalized anomalies), we have applied to the daily MUSt and LSt O_3 time series, a MLR model that is similar to that previously developed for tropospheric O_3 studies from IASI (see Eq. 1 and 2 in Wespes et al., 2017; 2018) but here adapted to fit the stratospheric variations. In addition to harmonic terms that represent

198 the 1-yr and 6-month variations, the MLR model includes the anthropogenic O_3 response through
199 a linear trend (LT) term and a set of explanatory variables (commonly called "proxies") to
200 parameterize the geophysical processes influencing the abundance of O_3 in the stratosphere. The
201 MLR uses an iterative stepwise backward elimination approach to retain, at the end of the
202 iterations, the most relevant proxies (with a 95% confidence level) explaining the O_3 variations
203 (e.g. Mäder et al., 2007). Table 1 lists the selected proxies, their sources and their temporal
204 resolutions. The proxies describe the influence of the Quasi-Biennial Oscillation (QBO; visible
205 from the deseasonalized anomaly maps in Fig.1c with a typical band-like pattern around the
206 Equator) at 10 hPa and 30 hPa, of the North Atlantic and the Antarctic Oscillations (NAO and
207 AAO), of the El Niño/Southern Oscillation (ENSO), of the volcanic aerosols (AERO) injected
208 into the stratosphere, of the strength of the Brewer-Dobson circulation (BDC) with the Eliassen-
209 Palm flux (EPF), of the polar O_3 loss driven by the volume of polar stratospheric clouds (VPSC),
210 of the tropopause height variation with the geopotential height (GEO) and of mixing of
211 tropospheric and stratospheric air masses with the potential vorticity (PV). The main proxies in
212 terms of their influence on O_3 are illustrated in Fig. 2 over the period of the IASI mission. The
213 construction of the EPF, VPSC and AERO proxies, which are specifically used in this study, is
214 explained hereafter, while the description of the other proxies can be found in previous IASI
215 studies (Wespes et al., 2016; 2017).
216
217 The EPF proxy consists of the normalized upward component of the EP flux crossing 100 hPa
218 and spatially averaged over the 45°-75° latitude band for each hemisphere. The fluxes are
219 calculated from the NCEP/NCAR 2.5°x2.5° gridded daily reanalysis (Kalnay et al., 1996) over
220 the IASI decade. The VPSC proxy is based on the potential volume of PSCs given by the volume
221 of air below the formation temperature of nitric acid trihydrate (NAT) over 60°-90° north and
222 south and calculated from the ERA-Interim reanalysis and from the MLS climatology of nitric
223 acid (I. Wohltmann, private communication; Wohltmann et al., 2007; and references therein).
224 The PSC volume is multiplied by the EESC to account for the changes in the amount of
225 inorganic stratospheric chlorine that activates the polar ozone loss. The O_3 build-up and the polar
226 O_3 loss are highly correlated with wintertime accumulated EP flux and PSC volume, respectively
227 (Fusco and Salby, 1999; Randel et al., 2002; Fioletov and Shepherd, 2003 and Rex et al., 2004).
228 These cumulative EP flux and PSC effects on O_3 levels are taken into account by integrating the
229 EPF and VPSC proxies over time with a specific exponential decay time according to the
230 formalism of Brunner et al. (2006; see Eq. 4). We set the relaxation time scale to 3 months
231 everywhere, except during the wintertime build-up phase of O_3 in the extratropics (from October
232 to March in the N.H. and from April to September in the southern hemisphere - S.H.) when it is
233 set to 12 months. For EFP, it accounts for the slower relaxation time of extratropical O_3 in winter
234 due to its longer photochemical lifetime. For VPSC, the 12-month relaxation time accounts for a
235 stronger effect of stratospheric chorine on spring O_3 levels: the maximum of the accumulated
236 VPSC (Fig. 2) coincides with the maximum extent of O_3 hole that develops during springtime
237 and that lasts until November. Note that correlations between VPSC and EPF are possible since

the same method is used to build these cumulative proxies. VPSC and EPF are also dynamically anti-correlated to some extent since a strong BDC is connected with warm polar stratospheric temperatures and, hence, reduced PSC volume (e.g. Wohltmann et al., 2007).

The AERO proxy is derived from aerosol optical depth (AOD) of sulfuric acid only. That proxy consists of latitudinally averaged (22.5°N-90°N – AERO-N, 22.5°S-90°S – AERO-S and 22.5°S-22.5°N – AERO-Eq) extinction coefficients at 12 µm calculated from merged aerosol datasets (SAGE, SAM, CALIPSO, OSIRIS, 2D-model-simulation and Photometer; Thomason et al., 2018) and vertically integrated over the two IASI stratospheric O_3 columns (AERO-MUSt and AERO-LSt). Fig.2 shows the AERO proxies (AERO-N, AERO-S and AERO-Eq) corresponding to the AOD over the whole stratosphere (150-2 hPa), while Fig.3 represents the latitudinal distribution of the volcanic sulfuric acid extinction coefficients integrated over the whole stratosphere (top panel) and, separately, over the MUSt (middle panel) and the LSt (bottom panel) from 2005 to 2017. The AOD distributions indicate the need for considering one specific AERO proxy for each latitudinal band (AERO-N, AERO-S and AERO-Eq) and for each vertical layer (AERO-MUSt and AERO-LSt). Note that, as an alternative proxy to AERO, the surface area density of ambient aerosol, that represents the aerosol surface available for chemical reactions, has been tested, giving similar results.

Note also that, similarly to what has already been found for tropospheric O_3 from IASI (Wespes et al., 2016), several time-lags for ENSO (1-, 3- and 5-month lags; namely, ENSO-lag1, ENSO-lag3 and ENSO-lag5) are also included in the MLR model to account for a possible delay in the O_3 response to ENSO at high latitudes.

Finally, autocorrelation in the noise residual ε (t) (see Eq. 1 in Wespes et al., 2016) is accounted for in the MLR analysis with time lag of one day to yield the correct estimated standard errors for the regression coefficients. They are estimated from the covariance matrix of the regression coefficients and corrected at the end of the iterative process by the autocorrelation of the noise residual. The regression coefficients are considered significant if they fall in the 95% confidence level (defined by 2σ level). In the seasonal MLR, the main proxies ($x_j X_{norm,j}$; with x_j, the regression coefficient and $X_{norm,j}$ the normalized proxy) are replaced by four explanatory variables ($x_{spr} X_{norm,spr} + x_{sum} X_{norm,sum} + x_{fall} X_{norm,fall} + x_{wint} X_{norm,wint}$) for each grid cell (see Section 2.2 in Wespes et al., 2017). Hence, the seasonal MLR adjusts 4 coefficients (instead of one in the annual MLR) to account for the seasonal O_3 response to changes in the proxy. If that method avoids to over-constrain the adjustment by the year-round proxies and, hence, reduces the systematic errors, the smaller daily data points covered by the seasonal proxies translate to a lower significance of these proxies. This is particularly true for EPF and VPSC that compensate each other by construction. As a consequence, the annual MLR is performed first in this study

Atmos. Chem. Phys. Discuss., https://doi.org/10.5194/acp-2019-206
Manuscript under review for journal Atmos. Chem. Phys.
Discussion started: 16 April 2019

Atmospheric Chemistry and Physics Discussions

and, then, complemented with the seasonal one when it is found helpful for further interpreting the observations.

Figure 4 shows the latitudinal distributions of the O_3 columns in the two stratospheric layers over the IASI decade (first panels in Fig.4 a and b), as well as those simulated by the annual MLR regression model (second panels) along with the regression residuals (third panels). The root mean square error (*RMSE*) of the regression residual and the contribution of the MLR model into the IASI O_3 variations (calculated as $\frac{\sigma\left(O_3^{\text{Fitted\_model}}(t)\right)}{\sigma\left(O_3(t)\right)}$ where σ is the standard deviation relative to the regression model and to the IASI time series; bottom panels) are also represented (bottom panels). The results indicate that the model reproduces ~25-85% and ~35-95% of the daily O_3 variations captured by IASI in the MUSt and the LSt, respectively, and that the residual errors are generally lower than 10% everywhere for the two layers, except for the spring O_3 hole region in the LSt. The *RMSE* relative to the IASI O_3 time series are lower than 20 DU and 15 DU at global scale in the LSt and the MUSt, respectively, except around the S.H. polar vortex in the LSt (~30 DU). On a seasonal basis (figure not shown), the results are only slightly improved: the model explains from ~35-90% and ~45-95% of the annual variations and the *RMSE* are lower than ~12 DU and ~23 DU everywhere, in the MUSt and the LSt, respectively. These results verify that the MLR models (annual and seasonal) reproduce well the time evolution of O_3 over the IASI decade in the two stratospheric layers and, hence, that they can be used to identify and quantify the main O_3 drivers in these two layers (see Section 3).

The MLR model has also been tested on nighttime FORLI-O_3 measurements only and simultaneously with daytime measurements, but this resulted in a lower quality fit, especially in the MUSt over the polar regions. This is due to the smaller vertical sensitivity of IASI during nighttime measurements, especially over cold surface, which causes larger correlations between stratospheric and tropospheric layers (e.g. 40-60% at high northern latitudes versus ~10-20% for daytime measurements based on deseasonalized anomalies) and, hence, which mixes counteracted processes from these two layers. For this reason, only the results for the MLR performed on daytime measurements are presented and discussed in this paper.

3 Drivers of O_3 natural variations

Ascribing a recovery in stratospheric O_3 to a decline in stratospheric halogen species requires first identifying and quantifying natural cycles that may produce trend-like segments in the O_3 time series, in order to prevent any misinterpretation of those segments as signs of O_3 recovery. The MLR analysis performed in Section 2.2 that was found to give a good representation of the MUSt and LSt O_3 records shows distinctive relevant patterns for the individual proxies retained in the regression procedure, as represented in Fig. 5. The fitted drivers are characterized by

314 significant regional differences in their regression coefficients with regions of in-phase relation
315 (positive coefficients) or out-of-phase relation (negative coefficients) with respect to the IASI
316 stratospheric O_3 anomalies. The areas of significant drivers (in the 95% confidence limit) are
317 surrounded by non-significant cells when accounting for the autocorrelation in the noise residual.
318 Figures 6 a and b respectively represent the latitudinal distribution of the fitted regression
319 coefficients for the proxies showing latitudinal variation only in the O_3 response (namely, QBO,
320 EPF, VPSC, AERO and ENSO) and of the contribution of these drivers into the O_3 variability
321 (calculated as the product of the 2σ variability of each proxy by its corresponding fitted
322 coefficient, i.e. the 2σ variability of the adjusted signal of the proxies). The 2σ O_3 variability in
323 the IASI measurements and in the fitted MLR model are also represented (black and grey lines,
324 respectively). Figure 7 displays the same results as Fig. 6b but for the austral spring and winter
325 periods only (using the seasonal MLR).
326
327 The PV and GEO proxies are generally minor components (not shown here) with relative
328 contributions smaller than 10% and large standard errors (>80%), except in the tropics where the
329 contribution for GEO reaches 40% in the LSt due to the tropopause height variation. Each other
330 adjusted proxy (QBO, SF, EPF, VPSC, AERO, ENSO, NAO and AAO) is an important
331 contributor to the O_3 variations, depending on the layer, region, and season as described next:
332
333 1. QBO - The QBO at 10hPa and 30hPa are important contributors around the Equator for
334 the two stratospheric layers. It shows up a typical band-like pattern of high positive
335 coefficients confined equatorward of ~15°N/S where the QBO is known to be a dominant
336 dynamical modulation force associated with strong convective anomalies (e.g. Randel
337 and Wu, 1996; Tian et al., 2006; Witte et al., 2008). In that latitude band, QBO10 and
338 QBO30 explain up to ~8 DU and ~5 DU, respectively, of the MUSt and LSt yearly O_3
339 variations (see Fig. 5 and 6b; i.e. relative contributions up to ~50% and ~40% for
340 QBO10/30 in MUSt and LSt O_3, respectively). The QBO is also influencing O_3 variations
341 poleward of 60°N/S with a weaker correlation between O_3 and equatorial wind anomalies
342 as well as in the sub-tropics with an out-of-phase transition. That pole-to-pole QBO
343 influence results from the QBO-modulation of extra-tropical waves and its interaction
344 with the BDC (e.g. Fusco and Salby, 1999). A pronounced seasonal dependence is
345 observed in the out-of-phase sub-tropical O_3 anomalies in the MUSt, with the highest
346 amplitude oscillating between the hemispheres in their respective winter (~5 DU of O_3
347 variations explained by QBO10/30 at ~20°S during JJA and at ~20°N during DJF; see
348 Fig. 7b for the JJA period in the MUStn the DJF period is not shown), which is in
349 agreement with Randel and Wu (1996). The amplitude of the QBO signal is found to be
350 stronger for QBO30 than for QBO10 in the LSt, which is in good agreement with studies
351 from other instruments for the total O_3 (e.g. Baldwin et al., 2001; Steinbrecht et al., 2006;
352 Frossard et al., 2013; Coldewey-Egbers et al., 2014) and from IASI in the troposphere
353 (Wespes et al., 2017). The smaller amplitude of O_3 response to QBO10 in the LSt

compared to the MUSt is again in agreement with previous studies that reported changes in phase of the QBO10 response as a function of altitude with a positive response in the upper stratosphere and destructive interference in the mid-low stratosphere (Chipperfield et al., 1994; Brunner et al., 2006).

2. SF - In the MUSt layer, the solar cycle O_3 response is one of the strongest contributors and explains globally between ~2 and 15 DU of in-phase O_3 variations (i.e. higher O_3 records during maximum solar irradiance) with the largest amplitude over the highest latitude regions (see Fig. 5; relative contribution up to ~20%). The solar influence in LSt is more complex with regions of in-phase and out-of-phase O_3 variations. The impact of solar variability on stratospheric O_3 abundance is due to a combination of processes: a modification in the O_3 production rates in the upper stratosphere induced by changes in spectral solar irradiance (e.g. Brasseur et al., 1993), the transport of solar proton event-produced NO_y from the mesosphere down to the mid-low stratosphere where it decreases active chlorine and bromine and, hence, O_3 destruction (e.g. Jackman et al., 2000; Hood and Soukharev, 2006; and references therein) and its impact on the lower stratospheric dynamics including the QBO (e.g. Hood et al., 1997; Zerefos et al., 1997; Kodera and Kuroda, 2002; Hood and Soukharev, 2003, Soukharev and Hood, 2006). As for the QBO, the strong SF dependence at polar latitudes in the LSt with zonal asymmetry in the O_3 response reflects the influence of the polar vortex strength and of stratospheric warmings, and are in good agreement with previous results (e.g. Hood et al., 1997; Zerefos et al., 1997; Labitzke and van Loon, 1999; Steinbrecht et al., 2003; Coldewey-Egbers et al., 2014). It is also worth noting that because only one solar cycle is covered, the QBO and SF effects could not be completely separated because they have a strong interaction (McCormack et al., 2007).

3. EPF - The vertical component of the planetary wave Eliassen-Palm flux entering the lower stratosphere corresponds to the divergence of the wave momentum that drives the meridional residual Brewer-Dobson circulation. In agreement with previous studies (e.g. Fusco and Salby, 1999; Randel et al., 2002; Brunner et al., 2006), fluctuations in the BDC are shown to cause changes on stratospheric O_3 distribution observed from IASI: EPF largely positively contributes to the LSt O_3 variations at high latitudes of both hemispheres where O_3 is accumulated because of its long chemical lifetime, with amplitude ranging between ~20 and 100 DU (see Fig. 5 and 6; i.e. relative contribution of ~35-150%). The influence of the EPF decreases at lower latitudes where a stronger circulation induces more O_3 transported from the tropics to middle-high latitudes and, hence, a decrease in O_3 levels particularly below 20 km (Brunner et al., 2006). The influence of EP fluxes in the Arctic is the smallest in summer (see Fig.7; <~35 DU *vs* ~70 DU in fall; the two other seasons are not shown) due to the later O_3 build-up in polar vortices. In the S.H., because of the deployment of the O_3 hole, the EP influence is

smaller than in the N.H. and the seasonal variations are less marked. In the MUSt, the O_3 response attributed to variations in EPF is positive in both hemispheres, with a much lower amplitude than in the LSt (up to ~20-35 DU). The region of out-of-phase relation with negative EPF coefficients over the high southern latitudes (Fig. 5b) is likely attributable to the influence of VPSC that has correlations with EPF by construction (see Section 2.2).

4. VPSC - Identically to EPF, VPSC is shown to mainly contribute to O_3 variations in LSt over the polar regions (~55 DU or 40% in the N.H. *vs* ~60 DU or 85% in the S.H. on a longitudinal average; see Fig. 6b) but with an opposite phase (Fig. 5 and 6a). The amplitude of the O_3 response to VPSC reaches its maximum over the southern latitudes during the spring (~60 DU; see Fig.7a for the austral spring period), which is consistent with the role of PSCs on the polar O_3 depletion when there is sufficient sunlight. The strong VPSC influence found at high northern latitudes in fall (Fig. 7a) are likely due to compensation effects with EPF as pointed out above. Note also that the VPSC contribution into MUSt reflects the larger correlation between the two stratospheric layers over the southern polar region (Section 2.1, Fig. 1d).

5. AERO - Five important volcanic eruptions with stratospheric impact occurred during the IASI mission (Kasatochi in 2008, Sarychev in 2009, Nabro in 2011, Sinabung in 2014 and Calbuco in 2015; see Fig.3). The two major eruptions of the last decades, El Chichon (1982) and Mt. Pinatubo (1991), which have injected sulfur gases into the stratosphere, have been shown to enhance PSCs particle abundances (~15-25 km altitude), to remove NO_x (through reaction with the surface of the sulfuric aerosol to form nitric acid) and, hence, to make the ozone layer more sensitive to active chlorine (e.g. Hofmann et al., 1989; Hofmann et al., 1993; Portmann et al., 1996; Solomon et al., 2016). Besides this chemical effect, the volcanic aerosols also warm the stratosphere at lower latitudes through scattering and absorption of solar radiation, which further induces indirect dynamical effects (Dhomse et al., 2015; Revell et al., 2017). Even though the recent eruptions have been of smaller magnitude than El Chichon and Mt. Pinatubo, they produced sulphur ejection through the tropopause into the stratosphere (see Section 2.2, Fig.2 and Fig.3), as seen with AOD reaching $5x10^{-4}$ over the stratosphere (150-2 hPa), especially following the eruptions of Nabro (13.3°N, 41.6°E), Sinabung (3.1°N, 98.3°E) and Calbuco (41.3°S, 72.6°W). In the LSt, the regression supports an enhanced O_3 depletion over the Antarctic in presence of sulfur gases with a significantly negative annual O_3 response reaching ~25 DU (i.e. relative contribution of ~20% into O_3 variation; see Fig. 5b). On the contrary, enhanced O_3 levels in response to sulfuric acid are found in the MUSt with a maximum impact of up to10 DU (i.e. relative contribution of ~20% into the O_3 variation; see Fig. 5a) over the Antarctic. The change in phase in the O_3 response to AERO between the LSt (~15-25 km) and the MUSt (~25-40 km) over the Antarctic, as

well as between polar and lower latitudes in the LSt (see Fig.5 and 6a), agree well with the heterogeneous reactions on sulfuric aerosol surface which reduce the concentration of NO_x to form nitric acid, leading to enhanced O_3 levels above 25 km but leading to decreased O_3 levels due to chlorine activation below 25 km (e.g. Solomon et al., 1996). On a seasonal basis, the depletion due to the presence of sulfur gases reaches ~30 DU on a longitudinal average, over the S.H. polar region during the austral spring (see Fig.7a) highlighting the link between volcanic gases converted to sulfate aerosols and heterogeneous polar halogen chemistry.

6. NAO – The NAO is an important mode of global climate variability, particularly in northern winter. It describes large-scale anomalies in sea level pressure systems between the sub-tropical Atlantic (Azores; high pressure system) and sub-polar (Iceland; low pressure system) regions (Hurrell, 1995). It disturbs the location and intensity of the North Atlantic jet stream that separates these two regions depending on the phase of NAO. The positive (negative) phase of the NAO corresponds to larger (weaker) pressure difference between the two regions leading to stronger westerlies (easterlies) across the mid-latitudes (Barnston and Livezey, 1987). The two pressure system regions are clearly identified in the stratospheric O_3 response to NAO, particularly in the LSt, with positive regression coefficients above the Labrador-Greenland region and negative coefficients above the Euro-Atlantic region (Fig. 5b). Above these two sectors, the positive phase induces, respectively, an increase and a decrease in LSt O_3 levels. The negative phase is characterized by the opposite behaviour. That NAO pattern is in line with previous studies (Rieder et al., 2013) and was also observed from IASI in tropospheric O_3 (Wespes et al., 2017). The magnitude of annual LSt O_3 changes attributed to NAO variations reaches ~20 DU over the in-phase Labrador region (i.e. contribution of 25% relative to the O_3 variations), while a much lower contribution is found for the MUSt (~4 DU or ~10%). The NAO coeffficient in the LSt also shows that the influence of the NAO extends further into northern Asia in case of prolonged NAO phases. The NAO has also been shown to influence the propagation of waves into the stratosphere, hence, the BDC and the strength of the polar vortex in the N.H. mid-winter (Thompson and Wallace, 2000; Schnadt and Dameris, 2003; Rind et al., 2005). That connection between the NAO and the BDC might explain the negative anomaly in the O_3 response to EPF in the LSt over northern Asia which matches the region of negative response to the NAO.

7. AAO - The extra-tropical circulation of the S.H. is driven by the Antarctic oscillation that is characterized by geopotential height anomalies south of 20°S, with high anomalies of one sign centered in the polar region and weaker anomalies of the opposing sign north of 55°S (Thompson and Wallace, 2000). This corresponds well to the two band-like regions of opposite signs found for the regression coefficients of adjusted AAO in the LSt (negative coefficients centered in Antarctica and positive coefficient north of ~40°S; see

Fig.5b). Similarly to the N.H. mode, the strength of the residual mean circulation and of the polar vortex in the S.H. are modulated by the AAO through the atmospheric wave activity (Thompson and Wallace, 2000; Thompson and Salomon, 2001). During the positive (negative) phase of the AAO, the BDC is weaker (stronger) leading to less (more) O_3 transported from the tropics into the southern polar region, and the polar vortex is stronger (weaker) leading to more (less) O_3 depletion inside. This likely explains both the positive AAO coefficients in the region north of ~40°S (contribution < ~5 DU or ~10%) and the negative coefficients around and over the Antarctic (contribution reaching ~10 DU or ~15%; exception is found with positive coefficients over the western Antarctic). The dependence of O_3 variations to the AAO in the MUSt is lower than ~7 DU (or ~15%).

8. ENSO - Besides the NAO and the AAO, the El Nino southern oscillation is another dominant mode of global climate variability. This coupled ocean-atmosphere phenomenon is governed by sea surface temperature (SST) differences between high tropical and low extra-tropical Pacific regions (Harrison and Larkin, 1998). Domeisen et al. (2019) have recently reviewed the possible mechanisms connecting the ENSO to the stratosphere in the tropics and the extratropics of both hemispheres. The ozone response to ENSO is represented in Fig. 5 only for the ENSO-lag3 proxy which is found to be the main ENSO proxy contributing to the observed O_3 variations. While in the troposphere, previous works have shown that the ENSO influence mainly results in a high contrast of the regression coefficients between western Pacific/Indonesia/North Australia and central/eastern Pacific regions caused by reduced rainfalls and enhanced O_3 precursor emissions above western Pacific (called “chemical effect”) (e.g. e.g. Oman et al., 2013; Valks et al., 2014; Ziemke et al., 2015; Wespes et al., 2016; and references therein), the LSt O_3 response to ENSO is shown here to translate into a strong tropical-extratropical gradient in the regression coefficients with a negative response in the tropics and a positive response at higher latitudes (~5 DU and ~10 DU, respectively, on longitudinal averages; see Fig. 6a). In the MUSt, ENSO is globally a smaller out-of-phase driver of O_3 variations (response of ~5 DU). The decrease in LSt O_3 during the warm ENSO phase in the tropics (characterized by a negative ENSO lag-3 coefficient reaching 7 DU (or 35%), respectively, in the LSt; see Fig. 5) is consistent with the ENSO-modulated upwelling via deep convection in the tropical lower stratosphere and, hence, increased BD circulation (e.g. Randel et al., 2009). The in-phase accumulation of LSt O_3 in the extra-tropics (contribution reaching 15 DU or 20%; see Fig. 5) is also consistent with enhanced extra-tropical planetary waves that propagate into the stratosphere during the warm ENSO phase, resulting in sudden stratospheric warmings and, hence, in enhanced BDC and weaker polar vortices (e.g. Brönnimann et al., 2004; Manzini et al., 2006; Cagnazzo et al., 2009). The very pronounced link between stratospheric O_3 and the ENSO related dynamical pathways with a time lag of about 3 months is one key finding of the present

work. Indeed, if the influence of ENSO on stratospheric O_3 measurements has been reported in earlier studies (Randel and Cobb, 1994; Brönnimann et al., 2004; Randel et al., 2009; Randel and Thompson, 2011; Oman et al., 2013; Manatsa and Mukwada, 2017; Tweedy et al., 2018), it is the first time that a delayed stratospheric O_3 response is investigated in MLR studies. A 4- to 6-month time lag in O_3 response to ENSO has similarly been identified from IASI in the troposphere (Wespes et al., 2017), where it was explained not only by a tropospheric pathway but also by a specific stratospheric pathway similar to that modulating stratospheric O_3 but with further impact downward onto tropospheric circulation (Butler et al., 2014; Domeisen et al., 2019). Furthermore, the 3-month lag identified in the LSt O_3 response is fully consistent with the modelling work of Cagnazzo et al. (2009) that reports a warming of the polar vortex in February-March following a strong ENSO event (peak activity in November-December) associated with positive O_3 ENSO anomaly reaching ~10 DU in the Arctic and negative anomaly of ~6-7 DU in the Tropics. We find that the tropical-extra-tropical gradient in O_3 response to ENSO-lag3 is indeed much stronger in spring with contributions of ~20-30 DU (see Fig.7a for the austral spring period *vs* winter).

Overall, although the annual MLR model underestimates the O_3 variability at high latitudes (>50°N/S) by up to 5 DU, particularly in the MUSt (see Fig. 6b), we conclude that it gives a good overall representation of the sources of O_3 variability in the two stratospheric layers sounded by IASI. This is particularly true for the spring period (see Fig. 7) which was studied in several earlier works to reveal the onset of Antarctic total O_3 recovery (Salby et al., 2011; Kuttippurath et al., 2013; Shepherd et al., 2014; Solomon et al., 2016; Weber et al., 2018), despite the large O_3 variability due to the hole formation during that period (~80 DU). It is also interesting to see from Fig.7 that the broad O_3 depletion over Antarctica in the LSt is attributed by the MLR to VPSC (up to 60 DU of explained O_3 variability on a latitudinal average). Following these promising results, we further analyze below the O_3 variability in response to anthropogenic perturbations, assumed in the MLR model by the linear trend term, with a focus over the polar regions.

4 Trend analysis

4.1 10-year trend detection in stratospheric layers

The distributions of the linear trend estimated by the annual regression are represented in Fig. 8a for the MUSt and the LSt (left and right panels). In agreement with the early signs of O_3 recovery reported for the extra-tropical mid- and upper stratosphere above ~25-10 hPa (>25-30 km; Pawson et al., 2014; Harris et al., 2015; Steinbrecht et al., 2017; Sofieva et al., 2017; Ball et al., 2018), the MUSt shows significant positive trends larger than 1 DU/yr poleward of ~35°N/S. The corresponding decadal trends (>10 DU/dec) are much larger than the discontinuity of ~2-4

554 DU encountered in the MUSt record on 15 September 2010 and discussed in section 2.1. The
555 tropical MUSt also shows positive trends but they are weaker (<0.8 DU/yr) or not significant.
556 The largest increase is observed in polar O_3 with amplitudes reaching ~2.5 DU/yr. The mid-
557 latitudes also show significant O_3 enhancement which can be attributed to airmass mixing after
558 the disruption of the polar vortex (Knudsen and Grooss, 2000; Fioletov and Shepherd, 2005;
559 Dhomse, 2006; Nair et al., 2015).
560
561 As in the MUSt, the LSt is characterized in the southern polar latitudes by significantly positive
562 and large trends (between ~ |1.0| and |2.5| DU/yr). In the mid-latitudes, the lower stratospheric
563 trends are significantly negative, i.e. opposite to those obtained in the MUSt. This highlights the
564 independence between the two O_3 layers sounded by IASI in the stratosphere. Poleward of 25°N
565 the negative LSt trends range between ~ |0.5| and |2.0| DU/yr. Negative trends in lower
566 stratospheric O_3 have already been reported in extra-polar regions from other space-based
567 measurements (Kyrölä et al., 2013; Gebhardt et al., 2014; Sioris et al., 2014; Harris et al., 2015;
568 Nair et al., 2015; Vigouroux et al., 2015; Wespes et al., 2016; Steinbrecht et al., 2017; Ball et al.,
569 2018) and may be due to changes in stratospheric dynamics at the decadal timescale (Galytska et
570 al., 2019). These previous studies, which were characterized by large uncertainties or resulted
571 from composite-data merging techniques, are confirmed here using a single dataset. The negative
572 trends which are observed at lower stratospheric middle latitudes are difficult to explain with
573 chemistry-climate models (Ball et al., 2018). It is also worth noting that the significant MUSt and
574 LSt O_3 trends are of the same order as those previously estimated from IASI over a shorter
575 period (from 2008 to 2013) and latitudinal averages (see Wespes et al., 2016). This suggests that
576 the trends are not very sensitive to the natural variability in the IASI time series, hence,
577 supporting the significance of the O_3 trends presented here.
578
579 The sensitivity of IASI O_3 to the estimated trend from MLR is further verified in Fig. 8b that
580 represents the global distributions of relative differences in the *RMSE* of the regression residuals
581 obtained with and without a linear trend term included in the MLR model ($(RMSE_{\_w/o\_LT} -$
582 $RMSE_{\_with\_LT})/RMSE_{\_with\_LT} \times 100$; in %). An increase of 1.0-4.0% and 0.5-2.0% in the *RMSE* is
583 indeed observed for both the MUSt and the LSt, respectively, in regions of significant trend
584 contribution (Fig. 8a), when the trend is excluded. This demonstrates the significance of the
585 trend in improving the performance of the regression. Another statistical method that can be used
586 for evaluating the possibility to infer, from the IASI time period, the significant positive or
587 negative trends in the MUSt and the LSt, respectively, consists in determining the expected year
588 when these specified trends would be detectable from the available measurements (with a
589 probability of 90%) by taking into account the variance (σ_ε^2) and the autocorrelation (Φ) of the
590 noise residual according to the formalism of Tiao et al. (1990) and Weatherhead et al. (1998). It
591 represents a more drastic and conservative method than the standard MLR. The results are
592 displayed in Fig. 8c for an assumed specified trend of |1.5| DU/yr, which corresponds to a

593 medium amplitude of trends derived here above from the MLR over the mid-polar regions (Fig.
594 8a). In the MUSt, we find that ~2-3 additional years of IASI measurements would be required to
595 unequivocally detect a positive trend of |1.5| DU/yr (with probability 0.90) over high latitudes
596 (detectable from ~2020-2022 ± 6-12 months) whereas it should already be detectable over the
597 mid- and lower latitudes (from ~2015 ± 3-6 months). In the LSt, additional ~7 years (± 1-2
598 years) of IASI measurement would be required to categorically identify the probable decline
599 derived from the MLR in northern mid-latitudes, and even more to measure the enhancement in
600 the southern polar latitudes. The longest required measurement period over the high latitudes is
601 explained by the largest noise residual (i.e. largest σ_ε) in the IASI data (see Fig.4 a and b). Note
602 that a larger specified trend amplitude would obviously require a shorter period of IASI
603 measurement. Only ~2 additional years would be required to detect a specified trend of |2.5|
604 DU/yr which characterizes the LSt at mid-high latitudes.
605
606 **4.2 Stratospheric contributions to total O_3 trend**
607
608 The effect on total O_3 of the counteracting trends in the northern mid-latitudes and of the
609 constructive trends in the southern polar latitudes trends derived in the two stratospheric layers
610 sounded by IASI is now investigated.
611
612 Figure 9 represents the global distributions of the contribution of the MUSt and the LSt into the
613 total O_3 columns (Fig.9a; in %), of the adjusted trends for the total O_3 (Fig. 9b in DU/yr) and of
614 the estimated year for a |15| DU per decade trend detection with a probability of 90% (Fig. 9c).
615 While no significant change or slightly positive trends in total O_3 after the inflection point in
616 1997 have been reported on an annual basis (e.g; Weber et al., 2018), Fig. 9b shows clear
617 significant changes: negative trend at northern mid-latitudes (up to ~2.0 DU/yr north of 30°N)
618 and positive trend over the southern polar region (up to ~3.0 DU/yr south of 40°S). Although
619 counteracting trends between lower and upper stratospheric O_3 have been pointed out in the
620 recent study of Ball et al. (2018) to explain the non-significant recovery in total O_3, we find from
621 IASI a dominance of the LSt decline that translates to negative trends over some regions of the
622 N.H. in TOC (Fig. 9b). This is explained by the contributions of 45-55% from the LSt to the total
623 column, *vs* ~30-40% from the MUSt (Fig. 9a) in the mid- and polar regions over the whole year.
624 In addition, the significant positive trends over the high southern latitudes in both the MUSt and
625 the LSt explains the largest total O_3 enhancement in polar region. Note that most previous ozone
626 trends studies, including Ball et al. (2018), excluded the polar regions due to limited latitude
627 coverage of some instruments merged in the data composites.
628
629 While the annual MLR shows a significant dominance of LSt trends over MUSt trends in the
630 northern mid-latitudes and significant constructive trends in the southern latitudes, total O_3
631 trends are not ascribed with complete confidence according to the formalism of Tiao et al. (1990)

and Weatherhead et al. (1998) discussed in Section 4.1. The detectability of a specified trend of |1.5| DU/yr (Fig. 9c), which corresponds to the medium trend derived from MLR in mid-high latitudes of both hemispheres (Fig. 9b), would need several years of additional measurements to be unequivocal from IASI on an annual basis (from ~2022-2024 over the mid-latitudes and from ~2035 over the polar regions). The highest trend amplitude of ~|2.5| DU/yr derived from the MLR would be observable from ~2020-2025 (figure not shown).

The use of the annual MLR could translate to large systematic uncertainties on trends (implying large σ_ε), which induces a longer measurement period required to yield significant trends. These uncertainties could be reduced on a seasonal basis, by attributing different weights to the seasons, which would help in the categorical detection of a specified trend. This is investigated in the subsection below by focusing on the winter and the spring periods.

4.3 Trends in polar spring

The reports on early signs of total O_3 recovery (Salby et al., 2011; Kuttippurath et al., 2013; Shepherd et al., 2014; Solomon et al., 2016; Kuttippurath and Nair, 2017; Weber et al., 2018) have all focused on the Antarctic region during spring, when the ozone hole area is at its maximum extent, i.e. the LSt O_3 levels at minimum values. Here we investigate the respective contributions of the LSt and the MUSt to the TOC recovery over the South Pole, looking also at the JJA period because the minima in O_3 levels in the MUSt over Antarctica occur later in summer (down to ~80 DU; see Fig.4a). Figures 10 and 11, respectively, show the S.H. and the N.H. distribution of the estimated trends from seasonal MLR (left panels) and of the corresponding year required for a significant detection of |30| DU increase per decade (right panels) during their respective winter (JJA and DJF; Fig. 10a and 11a) and spring (SON and MAM; Fig. 10b and 11b) for the total, MUSt and LSt O_3 (top, middle and bottom panels, respectively). Fig. 10 a and b clearly show significant positive trends over Antarctica and the southernmost latitudes of the Atlantic and Indian oceans, with amplitudes ranging between ~1-5 DU/yr over latitudes south of ~35-40°S in total, MUSt and LSt O_3 (~3.9±1.7 DU/yr, ~2.7±1.0 DU/yr, ~3.3±2.6 DU/yr and ~4.4±1.9 DU/yr, ~1.6±0.6 DU/yr, ~3.4±1.4 DU/yr, on spatial averages, respectively over JJA and SON, for the three O_3 columns). These trends are much larger than the amplitude of the discontinuity in the MUSt time series (section 2.1) and than the annual ones estimated in Sections 4.1 (see Fig.8 for the MUSt and the LSt) and 4.2 (see Fig.9 for TOC) over the whole year. In MUSt, significant positive trends are observed during each season over the mid- and polar latitudes of both hemispheres (Fig. 10 and 11 for the winter and spring periods; the other seasons are not shown here) but more particularly in winter and in spring where the increase reaches a maximum of ~ 4 DU/yr. In the LSt, the distributions are more complex: the trends are significantly negative in the mid-latitudes of both hemispheres, especially in winter, and in spring of the N.H., while in spring of the S.H., some mid-latitude

regions also show near-zero or even positive trends. The southern polar region shows high significant positive trends in winter/spring (see Fig.10). For the total O_3 at mid-high latitudes, given the mostly counteracting trends detected in the LSt and in the MUSt and the dominance of the LSt over the MUSt (~45-55% from the LSt vs ~30-40% from the MUSt into total O_3 over the whole year; except over the Antarctica in spring as discussed above), these latitudes are governed by negative trends with the highest decline in spring of the N.H. High significant increases are detected over polar regions in winter/spring of both hemispheres but more particularly in the S.H. where the LSt and MUSt trends are both of positive sign.

The substantial winter/spring positive trends observed in MUSt, LSt and total O_3 levels at high latitudes of the S.H. (and of the N.H. for the MUSt) are furthermore demonstrated to be detectable from the available IASI measurement period (see Fig. 10, right panels: an assumed increase of |3| DU/yr is detectable from 2016 ± 6 months and from 2018 ± 1 year in the MUSt and the LSt, respectively). The positive trend of ~4 DU/yr measured in polar total O_3 in winter/spring would be observable from ~2018-2020 ± 1-2 year and the decline of ~|3| DU/yr in winter/spring of the N.H. in LSt would be detectable from ~2018-2020 ± 9 months (not shown here). Note that the unrealistic negative trends found above the Pacific at highest latitudes (see Fig. 10) correspond to the regions with longest required measurement period for trend detection and, hence, point to poor regression residuals. About ~50% and ~35% of the springtime MUSt and LSt O_3 variations, respectively, are due to anthropogenic factors (estimated by VPSC×EESC proxy and linear trend in MLR models). This suggests that O_3 changes especially in the LSt are mainly governed by dynamics, which contributes to a later trend-detection year in comparison with the MUSt (Fig. 10 and 11) and which may hinder the O_3 recovery process.

Overall, the large positive trends estimated concurrently in LSt, MUSt and total O_3 over the Antarctic region in winter/spring likely reflect the healing of the ozone layer with a decrease of polar ozone depletion (Salomon et al., 2016) and, hence, demonstrate the efficiency of the Montreal protocol. To the best of our knowledge, these results represent the first detection of a significant recovery in the stratospheric and the total O_3 columns over the Antarctic from one single satellite dataset.

4.4 Speeding up in O_3 changes

Positive trends in total O_3 have already been determined earlier by Solomon et al. (2016) and by Weber et al. (2018) over Antarctica during September over earlier periods (~2.5±1.5DU/yr over 2000-2014 and 8.2±6.2%/dec over 2000-2016, respectively). The larger trends derived from the IASI records (Fig.10b; ~3.9±1.7 DU/yr on average) suggest that the O_3 response could be speeding up due to the accelerating decline of O_3 depleting substances (ODS) resulting from the Montreal Protocol. This has been investigated here by estimating the change in trend in MUSt, LSt and total O_3 over the IASI mission. Knowing that the length of the measurement period is an

important criterion for reducing systematic errors in the trend coefficient determination (i.e. the specific length of natural mode cycles should be covered to avoid any possible compensation effect between the covariates), the ozone response to each natural driver is taken from their adjustment over the whole IASI period (2008-2017; Section 3, Fig.5) and kept fixed. The linear trend term only is adjusted over variable measurement periods that all end in December 2017, by using a single linear iteratively reweighted least squares regression. The results are displayed in Fig. 12 for total, MUSt and LSt O_3 trends and their associated uncertainty (in the 95% confidence level) estimated from an annual regression. Note that the results are only shown for periods starting before 2015 as too short periods induce too large standard errors. In the LSt, a clear speeding up in the southern polar O_3 recovery is observed with amplitude ranging from ~1.5±0.3 DU/yr over 2008-2017 to ~6.5±3.5 DU/yr over 2015-2017 on latitudinal averages. Similarly, a speeding of the O_3 decline at northern mid-latitudes is found with values ranging between ~-0.7±0.2 DU/yr over 2008-2017 and ~-2.5±1.5 DU/yr over 2015-2017. In the MUSt, a weaker increase is observed over the year around ~60° latitude of the S.H. (from ~1.0±0.1 DU/yr over 2008-2017 to ~3.5±2.0 DU/yr over 2015-2017). Given the positive acceleration in both LSt and MUSt O_3 in the S.H., this is where the total O_3 record is characterized by the largest significant recovery (from ~1.5±0.3 DU/yr over 2008-2017 to ~8.5±3.5 DU/yr over 2015-2017). Surprisingly, the speeding up in the O_3 decline in the N.H. is more pronounced in the total O_3 (from ~-1.0±0.2 DU/yr over 2008-2017 to ~-3.5±1.5 DU/yr over 2015-2017) compared to the LSt, despite the opposite trend in MUSt O_3. This could reflect the O_3 decline observed in the northern latitudes in the troposphere (~|0.5| DU/yr over 2008-2016; cfr Wespes et al., 2018) which is included in the total column.

Overall, the larger annual trend amplitudes derived over the last few years of total, MUSt and LSt O_3 measurements, compared with those derived from the whole studied period (Sections 4.1 and 4.2) and from earlier studies translate to trends that are categorically detectable over the covered period. This demonstrates that we progress towards a significant emergence and speeding up of O_3 recovery process in the stratosphere over the whole year.

5 Summary and conclusion

In this study, we have analysed the changes in stratospheric O_3 levels sounded by IASI-A by examining the global pictures of natural and anthropogenic sources of O_3 changes independently in the lower (150-25 hPa) and in the mid-upper stratosphere (<25 hPa). We have exploited to that end a multi-linear regression model that has been specifically developed for the analysis of stratospheric processes by including a series of drivers known to have a causal relationship to natural stratospheric O_3 variations, namely SF, QBO-10, QBO-30, NAO, AAO, ENSO, AERO, EPF and VPSC. We have first verified the representativeness of the O_3 response to each of these natural drivers and found for most of them characteristic patterns that are in line with the current knowledge of their dynamical influence on O_3 variations. One of the most important finding

related to the O_3 driver analysis relied on the detection of a very clear time lag of 3 months in the O_3 response to ENSO in the LSt, with a pronounced contrast between an in-phase response in the extra-tropics and an out-of-phase response in the tropics, which is consistent with the ENSO-modulated dynamic. The 3-month lag observed in the lower stratosphere is also coherent with the 4- to -6 months lag detected from a previous study in the troposphere (Wespes et al., 2017) and further supports the stratospheric pathway suggested in Butler et al. (2014) to explain an ENSO influence over a long distance. The representativeness of the influence of the O_3 drivers was also confirmed on a seasonal basis (e.g. high ENSO-lag3 effect in spring, strong VPSC and AERO influences during the austral spring …). These results have verified the performance of the regression models (annual and seasonal) to properly discriminate between natural and anthropogenic drivers of O_3 changes. The anthropogenic influence has been evaluated with the linear trend adjustment in the MLR. The main results are summarized as follows:

(i) A highly probable (within 95%) recovery process is derived from the annual MLR at high southern latitudes in the two stratospheric layers and, therefore, in the total column. It is also derived at high northern latitudes in the MUSt. However, the effectiveness of the Montreal Protocol needs a longer period of IASI measurements for being unequivocally assured. Only ~2-3 additional years of IASI measurements are required in the MUSt.

(ii) A likely O_3 decline (within 95%) is measured in the lower stratosphere at mid-latitudes, specifically, of the N.H., but it would require an additional ~7 years of IASI measurements to be categorically confirmed. Given the large contribution from the LSt to the total column (~45-50% from LSt vs ~35% from the MUSt into TOCs), the decline is also calculated in total O_3 with ~4-6 years of additional measurements for being unequivocal.

(iii) A significant O_3 recovery is categorically found in the two stratospheric layers (>~35°N/S in the MUSt and >~45°S in the LSt) as well as in the total column (>~45°S) during the winter/spring period, which confirms previous studies that showed healing in the Antarctic O_3 hole with a decrease of its areal extent. These results verify the efficiency of the Montreal protocol with the banning of ODS, through the stratosphere and in the total column, from only one single satellite dataset for the first time.

(iv) The decline observed in LSt O_3 at northern mid-latitudes is unequivocal over the available IASI measurements in winter/spring of the N.H. The exact reasons for that decline are still unknown but O_3 changes in the LSt are estimated to be mainly attributable to dynamics and it likely perturbs the healing of LSt and total O_3 in the N.H.

(v) A significant speeding up (within 95%) in that decline is measured in LSt and total O_3 over the last 10 years (from ~-0.7±0.2 DU/yr over 2008-2017 to ~-2.5±1.5 DU/yr over 2015-2017 in LSt O_3 on latitudinal averages). It is of particular urgency to understand its causes for apprehending its possible impact on the O_3 layer and on future climate changes.

(vi) A clear and significant speeding up (within 95%) in stratospheric and total O_3 recovery is measured at southern latitudes (e.g. from ~1.5±0.3 DU/yr over 2008-2017 to ~6.5±3.5 DU/yr over 2015-2017 in the LSt) and translate to trend values that are categorically detectable on an annual basis. It demonstrates that we are currently progressing towards a substantial emergence in O_3 healing in the stratosphere over the whole year in the S.H..

Additional years of IASI measurements that will be provided by the operational IASI-C (2018) on flight and the upcoming IASI-Next Generation (IASI-NG) instrument onboard the Metop Second Generation (Metop-SG) series of satellites would be of particular interest to confirm and monitor, in a near future and over a longer period, the speeding up in the O_3 healing of the S.H. as well as in the LSt O_3 decline measured at mid-latitudes of the N.H. IASI-NG/Metop-SG is expected to extent the data record much further in the future (Clerbaux and Crevoisier, 2013; Crevoisier et al., 2014).

Author contribution

C.W. performed the analysis, wrote the manuscript and prepared the figures. D.H. was responsible for the retrieval algorithm development and the processing of the IASI O_3 dataset. S.C. and P.-F.C. contributed to the analysis. All authors contributed to the interpretation of the results and reviewed the manuscript.

Acknowledgments

IASI has been developed and built under the responsibility of the Centre National d'Etudes Spatiales (CNES, France). It is flown onboard the Metop satellites as part of the EUMETSAT Polar System. The IASI L1 data are received through the EUMETCast near real time data distribution service. We acknowledge the financial support from the ESA O_3-CCI and Copernicus O_3-C3S projects. FORLI-O_3 is being implemented at Eumetsat with the support of the AC SAF project. The research in Belgium is also funded by the Belgian State Federal Office for Scientific, Technical and Cultural Affairs and the European Space Agency (ESA Prodex IASI Flow and B-AC SAF). We acknowledge Ingo Wohltmann (Alfred Wagner Institute, Postdam, Germany) as well as Beiping Luo (Institute for Atmosphere and Climate, ETH Zurich,

Switzerland) and Larry Thomason (NASA Langley Research Center, Hampton, USA), for processing and providing datasets of volume of polar stratospheric clouds and of sulfuric acid extinction coefficients, respectively. We are also grateful to Maxime Prignon (Université de Liège, Liège, Belgium) for providing several years of BASCOE simulations.

Atmos. Chem. Phys. Discuss., https://doi.org/10.5194/acp-2019-206
Manuscript under review for journal Atmos. Chem. Phys.
Discussion started: 16 April 2019

Atmospheric Chemistry and Physics Discussions

871 **Table 1** List of the explanatory variables used in the multi-linear regression model applied on
872 IASI stratospheric O_3, their temporal resolution and their sources.
873

Proxy	Description (*resolution*)	Sources
F10.7	The 10.7 cm solar radio flux (*daily*)	NOAA National Weather Service Climate Prediction Center: ftp://ftp.ngdc.noaa.gov/STP/space-weather/solar-data/solar-features/solar-radio/noontime-flux/penticton/penticton_adjusted/listings/listing_drao_noontime-flux-adjusted_daily.txt
QBO^{10} **QBO^{30}**	Quasi-Biennial Oscillation index at 10hPa and 30hPa (*monthly*)	Free University of Berlin: www.geo.fu-berlin.de/en/met/ag/strat/produkte/qbo/
EPF	Vertical component of Eliassen-Palm flux crossing 100 hPa, averaged over 45°-75° for each hemisphere and accumulated over the 3 or 12 last months (see text for more details) (*daily*)	Calculated at ULB from the NCEP/NCAR gridded reanalysis: https://www.esrl.noaa.gov/psd/data/gridded/data.ncep.reanalysis.html
AERO	Stratospheric volcanic aerosols; Vertically integrated sulfuric acid extinction coefficient at 12 µm over 150-25 hPa and 25-2hPa, averaged over the tropics and the extra-tropics north and south (see text for more details) (*monthly*)	Extinction coefficients processed at the Institute for Atmosphere and Climate (ETH Zurich, Switzerland; Thomason et al., 2018)
VPSC	Volume of Polar Stratospheric Clouds for the N.H. and the S.H. multiplied by the equivalent effective stratospheric chlorine (EESC) and accumulated over the 3 or 12 last months (see text for details) (*daily*)	Processed at the Alfred Wagner Institute (AWI, Postdam, Germany; Ingo Wolthmann, private communication) EESC taken from the Goddard Space Flight Center: https://acd-ext.gsfc.nasa.gov/Data_services/automailer/index.html
ENSO	Multivariate El Niño Southern Oscillation Index (MEI) (2-*monthly averages*)	NOAA National Weather Service Climate Prediction Center: http://www.esrl.noaa.gov/psd/enso/mei/table.html
NAO	North Atlantic Oscillation index for the N.H. (*daily*)	ftp://ftp.cpc.ncep.noaa.gov/cwlinks/norm.daily.nao.index.b500101.current.ascii
AAO	Antarctic Oscillation index for the S.H. (*daily*)	ftp://ftp.cpc.ncep.noaa.gov/cwlinks/norm.daily.aao.index.b790101.current.ascii
GEO	Geopotential height at 200 hPa (*daily*)	http://apps.ecmwf.int/datasets/data/interim-full-daily/?levtype=pl
PV	Potential vorticity at 200 hPa (*daily*)	

874

Atmos. Chem. Phys. Discuss., https://doi.org/10.5194/acp-2019-206
Manuscript under review for journal Atmos. Chem. Phys.
Discussion started: 16 April 2019

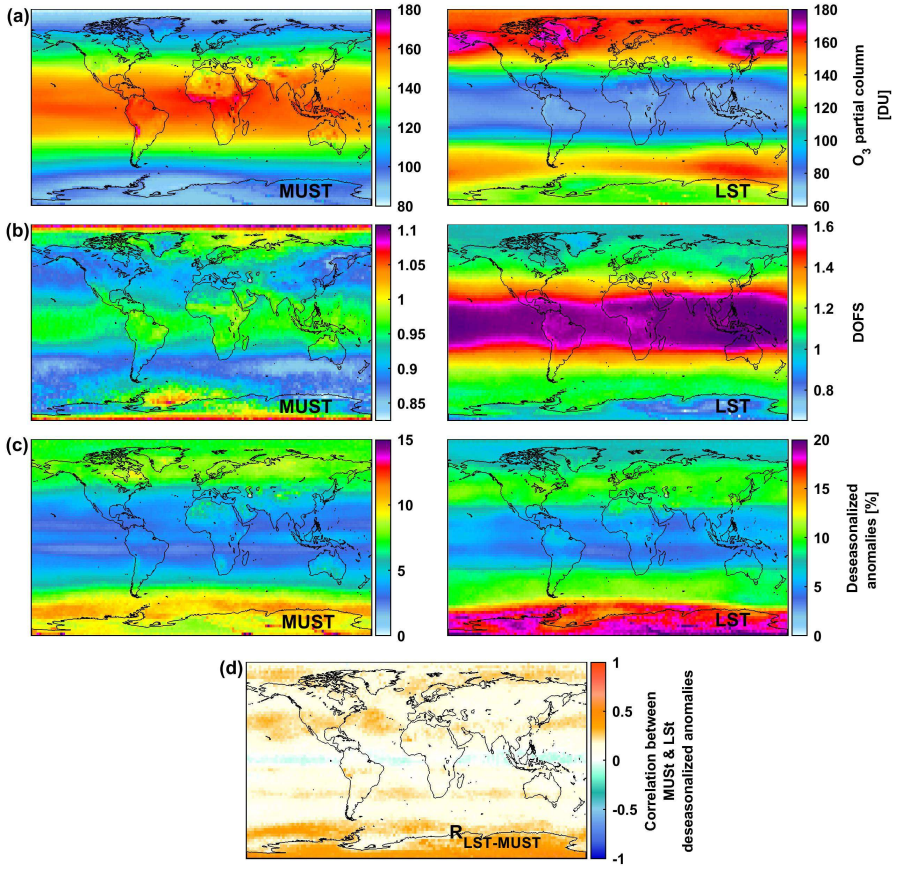

Fig.1. Global distribution of (a) daily O_3 columns (in Dobson Units - DU), (b) associated DOFS, (c) absolute deseasonalized anomalies (in %) averaged over January 2008 – December 2017 in the MUSt (Mid-Upper Stratosphere: >25 hPa; left panels) and in the LSt (Lower Stratosphere: 150-25hPa; right panels). (d) shows the correlation coefficients between the daily O_3 deseasonalized anomalies in the MUSt and in the LSt. Note that the scales are different between MUSt and LSt.

Atmos. Chem. Phys. Discuss., https://doi.org/10.5194/acp-2019-206
Manuscript under review for journal Atmos. Chem. Phys.
Discussion started: 16 April 2019

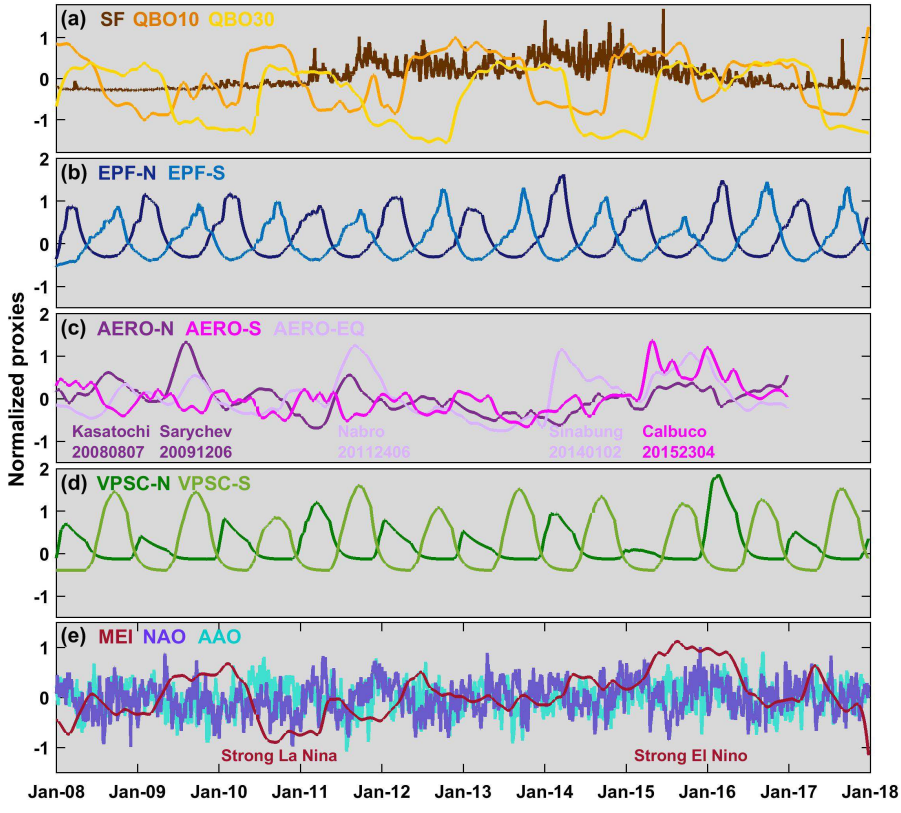

Fig.2. Normalized proxies as a function of time for the period covering January 2008 to December 2017 for (a) the F10.7 cm solar radio flux (SF) and the equatorial winds at 10 (QBO10) and 30 hPa (QBO30), respectively, (b) the upward components of the EP flux crossing 100 hPa accumulated over time and averaged over the 45°-75° latitude band for each hemispheres (EPF-N and EPF-S), (c) the extinction coefficients at 12 µm vertically integrated over the stratospheric O_3 column (from 150-2hPa) and averaged over the extra-tropics north and south (22.5°-90°N/S; AERO-N and AERO-S) and over the tropics (22.5°S-22.5°N; AERO-EQ) (the main volcanic eruptions are indicated), (d) the volume of polar stratospheric clouds multiplied by the equivalent effective stratospheric chlorine (EESC) and accumulated over time for the north and south hemispheres (VPSC-N and VPSC-S) and (e) the El Niño Southern (ENSO), North Atlantic (NAO) and Antarctic (AAO) oscillations.

Atmos. Chem. Phys. Discuss., https://doi.org/10.5194/acp-2019-206
Manuscript under review for journal Atmos. Chem. Phys.
Discussion started: 16 April 2019

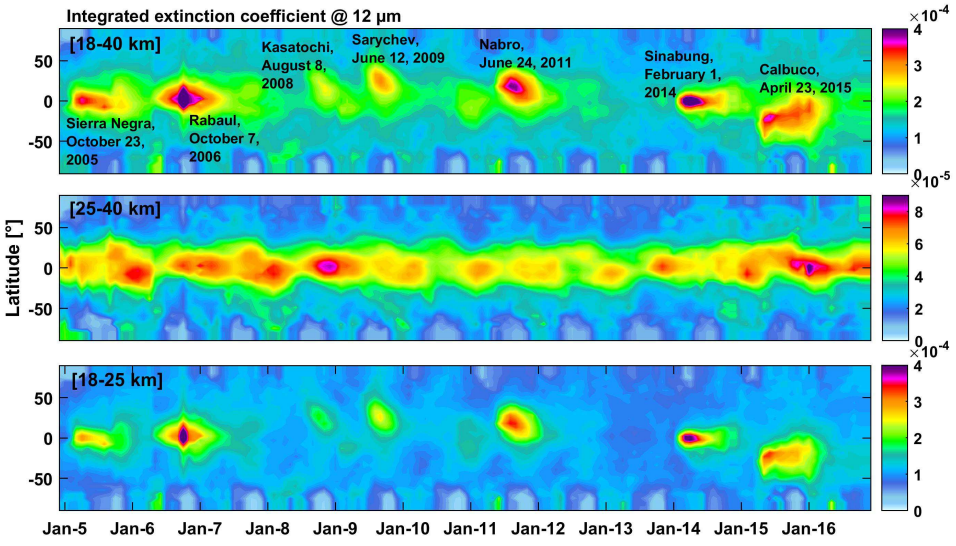

Fig.3: Latitudinal distribution of volcanic sulfuric acid extinction coefficient at 12 µm integrated over the stratosphere (top panel), over the middle stratosphere (middle panel) and the lower stratosphere (bottom panel) as a function of time from 2005 to 2017. The dataset consists of monthly mean aerosol data merged from SAGE, SAM, CALIPSO, OSIRIS, 2D-model-simulation and Photometer (processed at NASA Langley Research Center, USA and ETH Zurich, Switzerland).

Atmos. Chem. Phys. Discuss., https://doi.org/10.5194/acp-2019-206
Manuscript under review for journal Atmos. Chem. Phys.
Discussion started: 16 April 2019

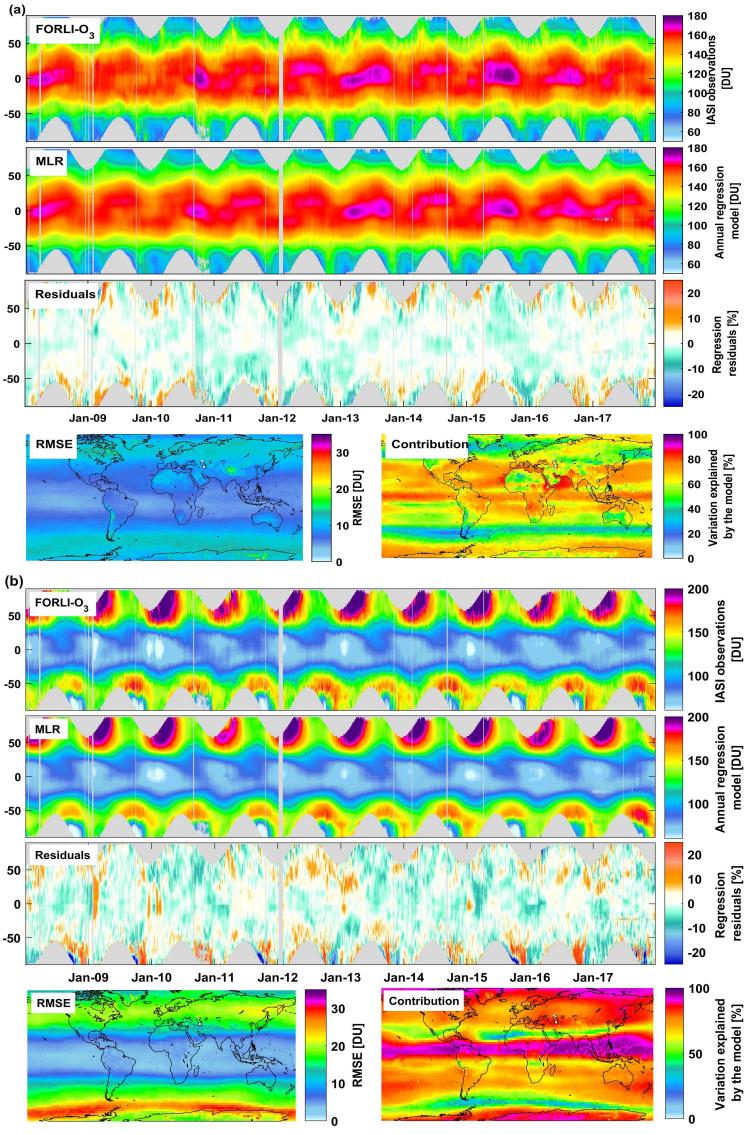

Fig.4: Latitudinal distribution of (a) MUSt O_3 column and (b) LSt O_3 columns as a function of time observed from IASI (in DU; top panels), simulated by the annual regression model (in DU, second panels) and of the regression residuals (in DU; third panels). Global distribution of *RMSE* of the regression residual (in DU) and fraction of the variation in IASI data explained by the regression model calculated as $\left[100\times\left(\sigma\left(O_3^{Fitted\_model}(t)\right)/\sigma\left(O_3(t)\right)\right)\right]$ (in %; fourth panels).

Atmos. Chem. Phys. Discuss., https://doi.org/10.5194/acp-2019-206
Manuscript under review for journal Atmos. Chem. Phys.
Discussion started: 16 April 2019

Atmospheric Chemistry and Physics Discussions

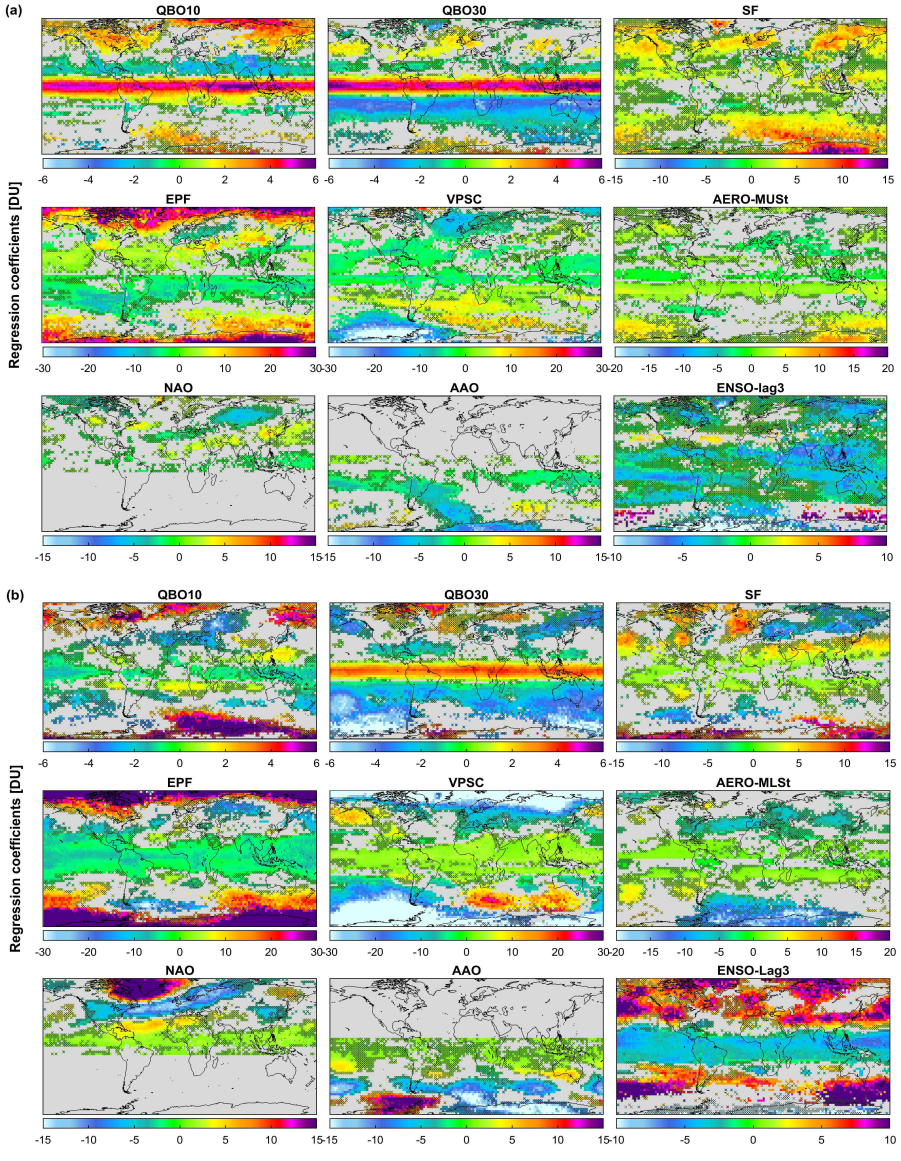

Fig.5: Global distribution of the annual regression coefficient estimates (in DU) for the main O_3 drivers in (a) MUSt and in (b) LSt: QBO10, QBO30, SF, EPF, VPSC, AERO, NAO, AAO and ENSO (ENSO-lag3 for both LSt and MUSt). Grey areas and crosses refer to non-significant grid cells in the 95% confidence limit. Note that the scales differ among the drivers.

Atmos. Chem. Phys. Discuss., https://doi.org/10.5194/acp-2019-206
Manuscript under review for journal Atmos. Chem. Phys.
Discussion started: 16 April 2019

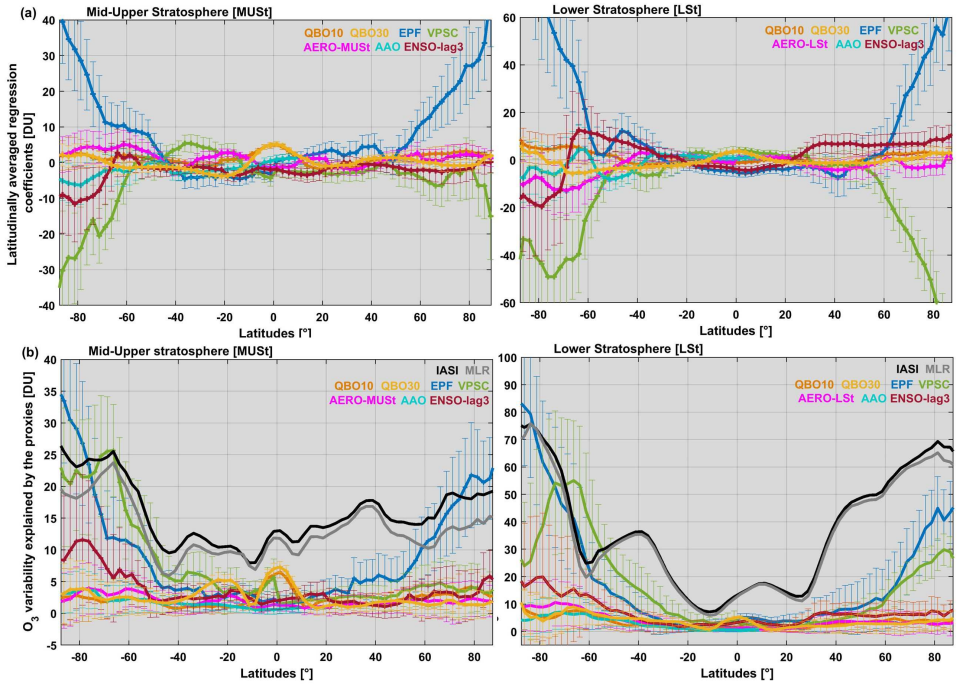

Fig.6: Latitudinal distributions (a) of fitting regression coefficients for various O_3 drivers (QBO10, QBO30, EPF, VPSC, AERO, AAO and ENSO-lag3; in DU) and (b) of 2σ O_3 variability due to variations in those drivers (in DU) from the annual MLR in MUSt and LSt (left and right panels respectively). Vertical bars correspond (a) to the uncertainty of fitting coefficients at the 2σ level and (b) to the corresponding error contribution into O_3 variation. Note that the scales are different.

Atmos. Chem. Phys. Discuss., https://doi.org/10.5194/acp-2019-206
Manuscript under review for journal Atmos. Chem. Phys.
Discussion started: 16 April 2019

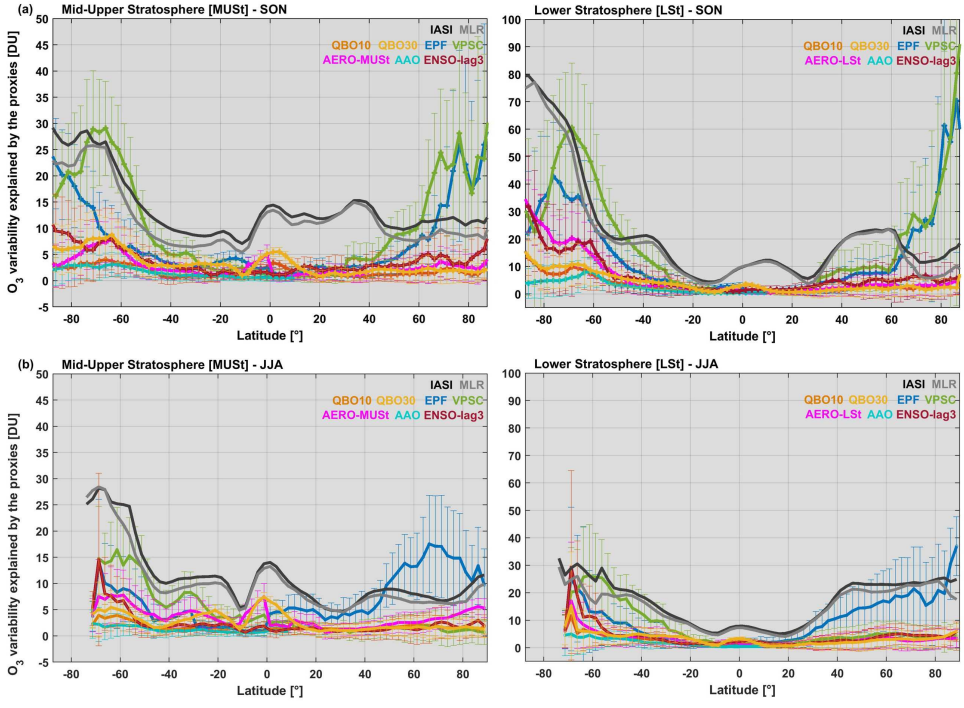

Fig.7: Same as Fig. 6b but for (a) the austral winter and (b) the austral spring periods (JJA and SON, respectively) from the seasonal MLR. Note that the scales are different.

Atmos. Chem. Phys. Discuss., https://doi.org/10.5194/acp-2019-206
Manuscript under review for journal Atmos. Chem. Phys.
Discussion started: 16 April 2019

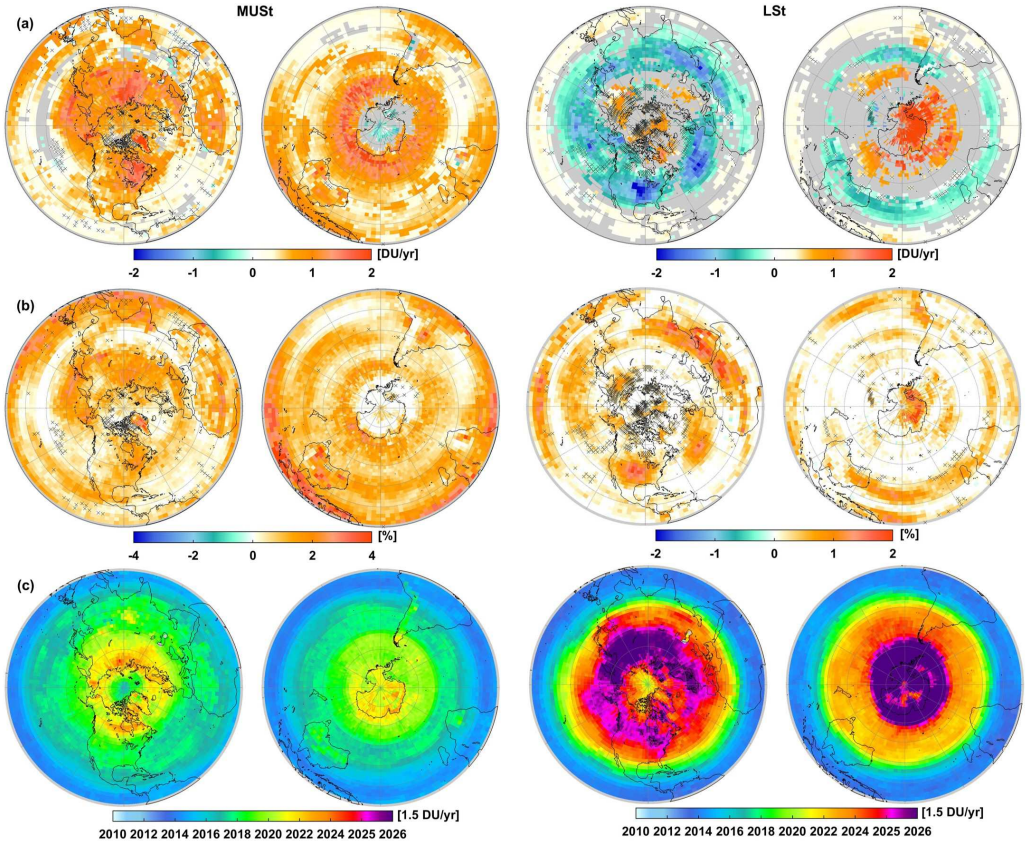

Fig. 8: Global distribution (a) of the estimated annual trends (in DU/yr; grey areas and crosses refer to non-significant grid cells in the 95% confidence limit), (b) of the IASI sensitivity to trend calculated as the differences between the *RMSE* of the annual MLR fits with and without linear trend term [$(RMSE_{\_w/o\_LT} - RMSE_{\_with\_LT})/RMSE_{\_with\_LT} \times 100$] (in %), (c) of the estimated year for a significant detection (with a probability of 90%) of a given trend of |1.5| DU/yr starting in January 2008 in MUSt and LSt O_3 columns (left and right panels, respectively). Note that the scales of panels (b) are different for the two layers.

Atmos. Chem. Phys. Discuss., https://doi.org/10.5194/acp-2019-206
Manuscript under review for journal Atmos. Chem. Phys.
Discussion started: 16 April 2019

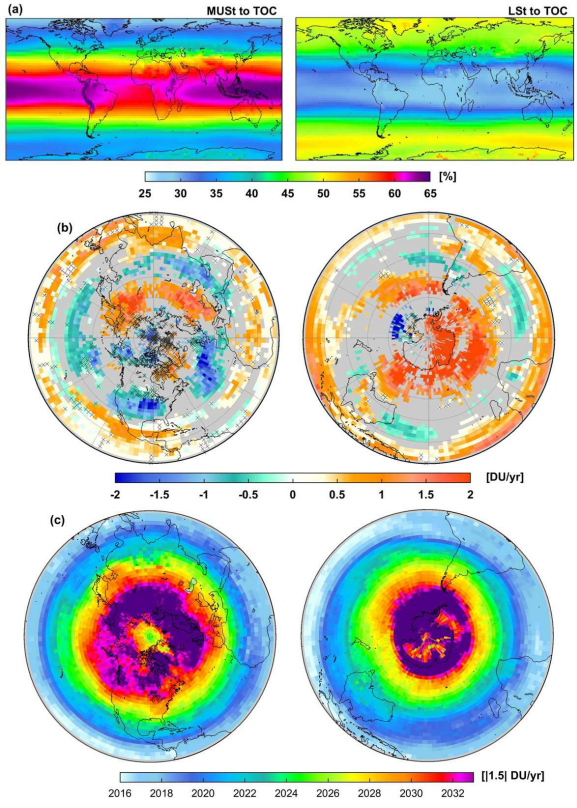

Fig.9: Global distribution of (a) the contribution (in %) of MUSt and LSt into the total O_3 (left and right panels respectively) averaged over January 2008 – December 2017, (b) fitted trends in total O_3 (in DU/yr; the grey areas and crosses refer to the non-significant grid cells in the 95% confidence limit) and (c) estimated year for the detection of a significant trend in total O_3 (with a probability of 90%) for a given trend of |1.5| DU/yr starting on January 2008.

Atmos. Chem. Phys. Discuss., https://doi.org/10.5194/acp-2019-206
Manuscript under review for journal Atmos. Chem. Phys.
Discussion started: 16 April 2019

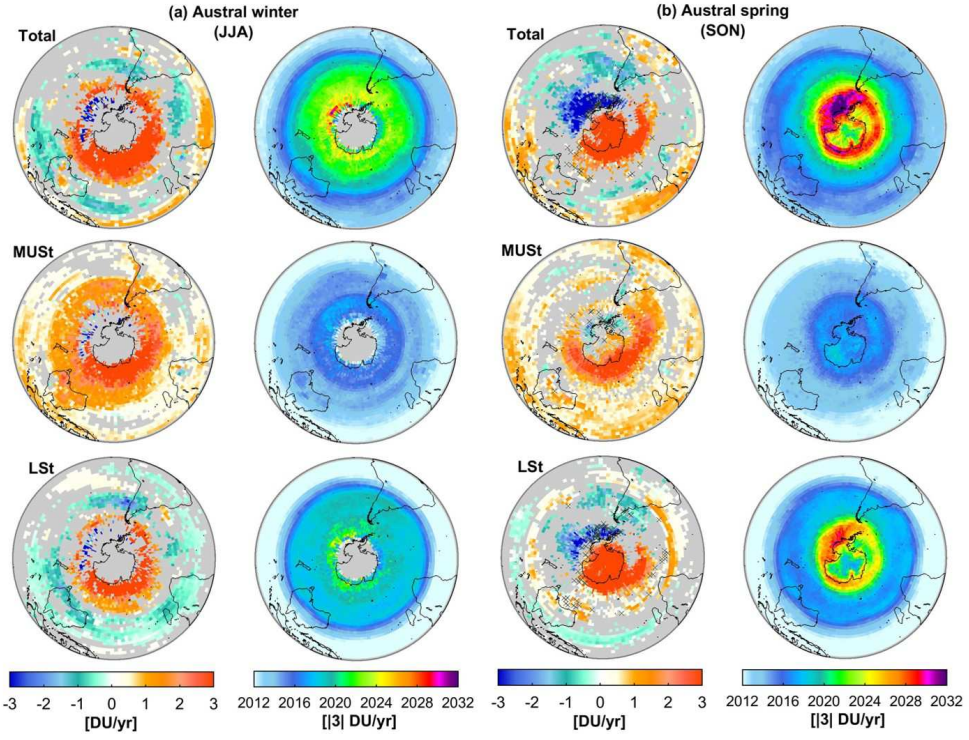

Fig.10: Hemispheric distribution (a) in austral winter (JJA) and (b) in austral spring (SON) of the estimated trends in total, MUSt and LSt O_3 columns (left panels: top, middle and bottom, respectively; in DU/yr; the grey areas and crosses refer to the non-significant grid cells in the 95% confidence limits) and of the corresponding estimated year for a significant trend detection (with a probability of 90%) of a given trend of |3| DU/yr starting at January 2008 (right panels: top, middle and bottom, respectively).

Atmos. Chem. Phys. Discuss., https://doi.org/10.5194/acp-2019-206
Manuscript under review for journal Atmos. Chem. Phys.
Discussion started: 16 April 2019

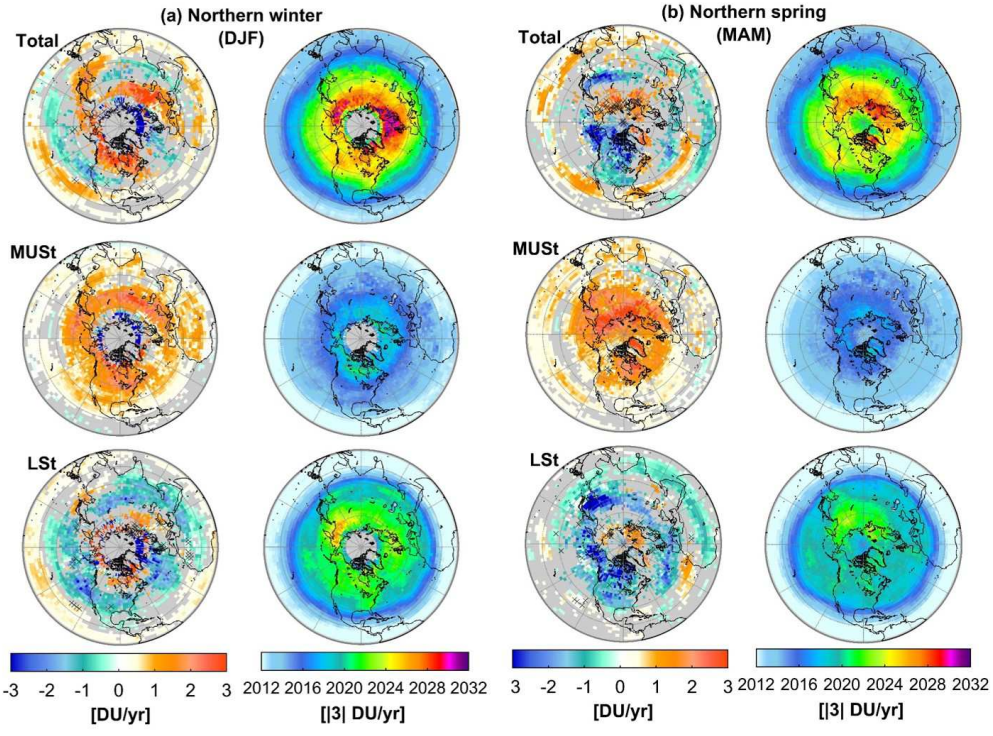

Fig. 11: Same as Fig. 10 but (a) for the winter (DJF) and (b) for the spring (MAM) of the northern Hemisphere.

Atmos. Chem. Phys. Discuss., https://doi.org/10.5194/acp-2019-206
Manuscript under review for journal Atmos. Chem. Phys.
Discussion started: 16 April 2019

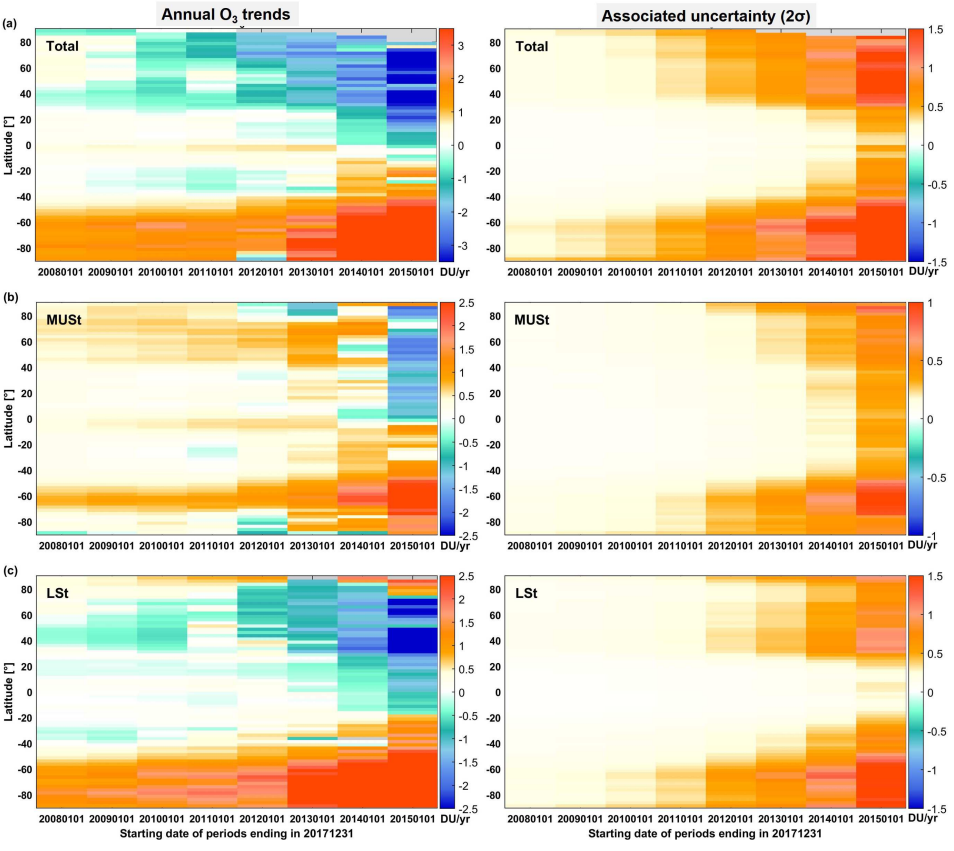

Fig.12: Evolution of estimated linear trend (DU/yr) and associated uncertainty (DU/yr; in the 95% confidence level) in (a) total, (b) MUSt and (c) LSt O_3 columns, as a function of the covered IASI measurement period ending in December 2017, with all natural contributions estimated from the whole IASI period (2008-2017). Note that the scales are different between the columns.

References

Anderson, J., Russell, J. M., Solomon, S., and Deaver, L. E.: Halogen Occultation Experiment confirmation of stratospheric chlorine decreases in accordance with the Montreal Protocol, J. Geophys. Res.-Atmos., 105, 4483–4490, https://doi.org/10.1029/1999JD901075, 2000.

Baldwin, M. P., L.J. Gray, T.J. Dunkerton, K. Hamilton, P.H. Haynes, W.J. Randel, J.R. Holton, M.J. Alexander, I. Hirota, T. Horinouchi, D.B.A. Jones, J.S. Kinnersley, C. Marquardt, K. Sato, and M. Takahashi: The quasi-biennial oscillation, Rev. Geophys., 39, 179–230, doi:10.1029/1999RG000073, 2001.

Ball, W. T., Alsing, J., Mortlock, D. J., Staehelin, J., Haigh, J. D., Peter, T., Tummon, F., Stübi, R., Stenke, A., Anderson, J., Bourassa, A., Davis, S. M., Degenstein, D., Frith, S., Froidevaux, L., Roth, C., Sofieva, V., Wang, R., Wild, J., Yu, P., Ziemke, J. R., and Rozanov, E. V.: Evidence for a continuous decline in lower stratospheric ozone offsetting ozone layer recovery, Atmos. Chem. Phys., 18, 1379–1394, https://doi.org/10.5194/acp-18-1379-2018, 2018.

Barnston, A. G. and Livezey, R. E.: Classification, seasonality and persistence of low-frequency atmospheric circulation patterns, Mon. Weather. Rev. 115: 1083–1126, 1987.

Boynard, A., D. Hurtmans, K. Garane, F. Goutail, J. Hadji-Lazaro, M. E. Koukouli, C. Wespes, C. Vigouroux, A. Keppens, J.-P. Pommereau, A. Pazmino, D. Balis, D. Loyola, P. Valks, R. Sussmann, D. Smale, P.-F. Coheur and C. Clerbaux: Validation of the IASI FORLI/Eumetsat O_3 products using satellite (GOME-2), ground-based (Brewer-Dobson, SAOZ, FTIR) and ozonesonde measurements, Atmos. Meas. Tech., 11, 5125–5152, 2018.

Brasseur, G.: The response of the middle atmosphere to long-term and short-term solar variability: A two-dimensional model, J. Geophys. Res., 98, 23 079–23 090, 1993.

Brönnimann, S., Luterbacher, J., Staehelin, J., Svendby, T. M., Hansen, G., and Svenøe, T.: Extreme climate of the global troposphere and stratosphere 1940–1942 related to El Nino, Nature, 431, 971–974, 2004.

Brunner, D., Staehelin, J., Maeder, J. A., Wohltmann, I., and Bodeker, G. E.: Variability and trends in total and vertically resolved stratospheric ozone based on the CATO ozone data set, Atmos. Chem. Phys., 6, 4985–5008, doi:10.5194/acp-6-4985-2006, 2006.

Buffet, L., Villaret, C., Jacquette, E., Vandermarcq, O., Astruc, P., and Anstötz, S.: Status of IASI instruments onboard Metop-A and Metop-B satellites, 4th IASI International Conference, Antibes Juan-Les-Pins, France, 11–15 April 2016, available at: https://iasi.cnes.fr/sites/default/files/drupal/201612/default/bpc_iasi-conference4-1_02_instruments_buffet.pdf (last access: 30 August 2018), 2016.

1057 Butler, A. H., M. Polvani, and C. Deser: Separating the stratospheric and tropospheric pathways
1058 of El Niño–Southern Oscillation teleconnections, Environ. Res. Lett., 9, 2, 024014,
1059 doi:10.1088/1748-9326/9/2/024014, 2014.
1060
1061 Cagnazzo, C., E. Manzini, N. Calvo, A. Douglass, H. Akiyoshi, S. Bekki, M. Chipperfield, M.
1062 Dameris, M. Deushi, A. M. Fischer, H. Garny, A. Gettelman, M. A. Giorgetta, D. Plummer, E.
1063 Rozanov, T. G. Shepherd, K. Shibata, A. Stenke, H. Struthers and W. Tian: Northern winter
1064 stratospheric temperature and ozone responses to ENSO inferred from an ensemble of Chemistry
1065 Climate Models, Atmos. Chem. Phys., 9, 8935–8948, www.atmos-chem-phys.net/9/8935/2009/,
1066 2009.
1067
1068 Chabrillat, S., Vigouroux, C., Christophe, Y., Engel, A., Errera, Q., Minganti, D., Monge-Sanz,
1069 B. M., Segers, A., and Mahieu, E.: Comparison of mean age of air in five reanalyses using the
1070 BASCOE transport model, Atmos. Chem. Phys., 18, 14715-14735, 2018.
1071
1072 Chipperfield, M. P., Kinnersley, J. S., and Zawodny, J.: A twodimensional model study of the
1073 QBO signal in SAGE II NO_2 and O_3, Geophys. Res. Lett., 21, 589–592, 1994.
1074
1075 Chubachi, S.: Preliminary results of ozone observations at Syowa Station from February 1982 to
1076 January 1983, in: Proc. Sixth Symposium on Polar Meteorology and Glaciology, edited by:
1077 Kusunoki, K., vol. 34 of Mem. National Institute of Polar Research Special Issue, 13–19, 1984.
1078
1079 Clarisse, L., Clerbaux, C., Franco, B., Hadji-Lazaro, J., Whitburn, S., Kopp, A. K., D. Hurtmans
1080 and P.-F. Coheur: A decadal data set of global atmospheric dust retrieved from IASI satellite
1081 measurements, J. Geophys. Res., 124, https://doi.org/10.1029/2018JD029701, 2019.
1082
1083 Coldewey-Egbers, M., D. G. Loyola R., P. Braesicke, M. Dameris, M. van Roozendael, C. Lerot,
1084 and W. Zimmer: A new health check of the ozone layer at global and regional scales, Geophys.
1085 Res. Lett., 41, 4363–4372, doi:10.1002/2014GL060212, 2014.
1086
1087 Clerbaux, C., A. Boynard, L. Clarisse, M. George, J. Hadji-Lazaro, H. Herbin, D. Hurtmans, M.
1088 Pommier, A. Razavi, S. Turquety, C. Wespes, and P.-F. Coheur: Monitoring of atmospheric
1089 composition using the thermal infrared IASI/MetOp sounder, Atmos. Chem. Phys., 9, 6041-
1090 6054, 2009.
1091
1092 Clerbaux, C. and Crevoisier, C.: New Directions: Infrared remote sensing of the troposphere
1093 from satellite: Less, but better, Atmos. Environ., 72, 24–26, 2013.
1094
1095 Cochrane, D. and Orcutt, G. H.: Application of least squares regression to relationships
1096 containing auto-correlated error terms, J. Am. Stat. Assoc., 44, 32–61, 1949.
1097
1098 Crevoisier, C., Clerbaux, C., Guidard, V., Phulpin, T., Armante, R., Barret, B., Camy-Peyret, C.,
1099 Chaboureau, J.-P., Coheur, P.-F., Crépeau, L., Dufour, G., Labonnote, L., Lavanant, L., Hadji-
1100 Lazaro, J., Herbin, H., Jacquinet-Husson, N., Payan, S., Péquignot, E., Pierangelo, C., Sellitto,
1101 P., and Stubenrauch, C. : Towards IASI-New Generation (IASI-NG): impact of improved

spectral resolution and radiometric noise on the retrieval of thermodynamic, chemistry and climate variables, Atmos. Meas. Tech., 7, 4367-4385, 2014.

Crutzen, P. J.: Estimates of possible future ozone reductions from continued use of fluoro-chloro-methanes (CF2Cl2, CFCl3), Geophys. Res. Lett., 1, 205–208, https://doi.org/10.1029/GL001i005p00205, 1974.

Dhomse, S., Weber, M., Wohltmann, I., Rex, M., and Burrows, J. P.: On the possible causes of recent increases in northern hemispheric total ozone from a statistical analysis of satellite data from 1979 to 2003, Atm. Chem. Phys., 6, 1165–1180, 2006.

Dhomse, S. S., Chipperfield, P., Feng, W., Hossaini, R., Mann G. W., and Santee, M. L.: Revisiting the hemispheric asymmetry in midlatitude ozone changes following the Mount Pinatubo eruption: A 3-D model study, Geophys. Res. Lett., 42, 3038–3047, 2015.

Domeisen, D. I., Garfinkel, C. I., and Butler, A. H.: The teleconnection of El Niño Southern Oscillation to the stratosphere, Reviews of Geophysics, 57. https://doi.org/10.1029/2018RG000596, 2019.

Farman, J. C., Gardiner, B. G., and Shanklin, J. D.: Large losses of total ozone in Antarctica reveal seasonal ClOx/NOx interaction, Nature, 315, 207–210, doi:10.1038/315207a0, 1985.

Fioletov, V. E. and Shepherd, T. G.: Seasonal persistence of midlatitude total ozone anomalies, Geophys. Res. Lett., 30, 1417, doi:10.1029/2002GL016739, 2003.

Fioletov, V. E. and Shepherd, T. G.: Summertime total ozone variations over middle and polar latitudes, Geophys. Res. Lett, 32, 4807, doi:10.1029/2004GL022080, 2005.

Fishman, J., J.K. Creilson, A.E. Wozniak, and P.J. Crutzen, The interannual variability of stratospheric and tropospheric ozone determined from satellite measurements, J. Geophys. Res., 110, D20306, doi:10.1029/2005JD005868, 2005.

Frossard, L., H.E. Rieder, M. Ribatet, J. Staehelin, J. A, Maeder, S. Di Rocco, A. C. Davison, T. Pete.: On the relationship between total ozone and atmospheric dynamics and chemistry at mid-latitudes – Part 1: Statistical models and spatial fingerprints of atmospheric dynamics and chemistry, Atmos. Chem. Phys., 13, 147–164, doi:10.5194/acp-13-147-2013, 2013.

Fusco, A. C. and Salby, M. L.: Interannual variations of total ozone and their relationship to variations of planetary wave activity, J. Clim., 12, 1619–1629, 1999.

Galytska, E., Rozanov, A., Chipperfield, M. P., Dhomse, Sandip. S., Weber, M., Arosio, C., Feng, W., and Burrows, J. P.: Dynamically controlled ozone decline in the tropical mid-stratosphere observed by SCIAMACHY, Atmos. Chem. Phys., 19, 767-783, https://doi.org/10.5194/acp-19-767-2019, 2019.

1147 Gebhardt, C., Rozanov, A., Hommel, R., Weber, M., Bovensmann, H., Burrows, J. P.,
1148 Degenstein, D., Froidevaux, L., and Thompson, A. M.: Stratospheric ozone trends and variability
1149 as seen by SCIAMACHY from 2002 to 2012, Atmos. chem. Phys., 14, 831–846,
1150 https://doi.org/10.5194/acp-14-831-2014, 2014.
1151
1152 Harris, N. R. P., Hassler, B., Tummon, F., Bodeker, G. E., Hubert, D., Petropavlovskikh, I.,
1153 Steinbrecht, W., Anderson, J., Bhartia, P. K., Boone, C. D., Bourassa, A., Davis, S. M.,
1154 Degenstein, D., Delcloo, A., Frith, S. M., Froidevaux, L., Godin-Beekmann, S., Jones, N.,
1155 Kurylo, M. J., Kyrölä, E., Laine, M., Leblanc, S. T., Lambert, J.-C., Liley, B., Mahieu, E.,
1156 Maycock, A., De Mazière, M., Parrish, A., Querel, R., Rosenlof, K. H., Roth, C., Sioris, C.,
1157 Staehelin, J., Stolarski, R. S., Stübi, R., Tamminen, J., Vigouroux, C., Walker, K. A., Wang, H.
1158 J., Wild, J., and Zawodny, J. M.: Past changes in the vertical distribution of ozone – Part 3:
1159 Analysis and interpretation of trends, Atmos. Chem. Phys., 15, 9965-9982,
1160 https://doi.org/10.5194/acp-15-9965-2015, 2015.
1161
1162 Harrison, D. E., and Larkin, N. K.: El Niño-Southern Oscillation sea surface temperature and
1163 wind anomalies, 1946–1993, Rev. Geophys., 36, 353–399, doi:10.1029/98RG00715, 1998.
1164
1165 Hilton, F., R. Armante, T. August, et al. : Hyperspectral Earth Observation from IASI: Five
1166 Years of Accomplishments, Bulletin of the American Meteorological Society, vol. 93, issue 3,
1167 pp. 347-370, 2012.
1168
1169 Hofmann, D. J. and Solomon, S.: Ozone destruction through heterogeneous chemistry following
1170 the eruption of El Chichón, J. Geophys. Res., 94, 5029,
1171 https://doi.org/10.1029/JD094iD04p05029, 1989.
1172
1173 Hofmann, D. J., S. J. Oltmans, Antarctic ozone during 1992: Evidence for Pinatubo volcanic
1174 aerosol effects. J. Geophys. Res. 98, 18555–18561, doi:10.1029/93JD02092, 1993.
1175
1176 Hofmann, D. J., S. J. Oltmans, J. M. Harris, B. J. Johnson, and J. A. Lathrop: Ten years of
1177 ozonesonde measurements at the south pole: Implications for recovery of springtime Antarctic
1178 ozone, J. Geophys. Res., 102(D7), 8931– 8943, doi:10.1029/96JD03749, 1997.
1179
1180 Hood, L. L., McCormick, J. P., and Labitzke, K.: An investigation of dynamical contributions to
1181 midlatitude ozone trends in winter, J. Geophys. Res, 102, 13 079–13 093, 1997.
1182
1183 Hood, L. L., and B. E. Soukharev: Quasi-decadal variability of the tropical lower stratosphere:
1184 The role of extratropical wave forcing, J. Atmos. Sci., 60, 2389–2403, 2003.
1185
1186 Hood, L. L., and B. E. Soukharev: Solar induced variations of odd nitrogen: Multiple regression
1187 analysis of UARS HALOE data, Geophys. Res. Lett., doi:10.1029/2006GL028122, 2006.
1188
1189 Hubert, D., Lambert, J.-C., Verhoelst, T., Granville, J., Keppens, A., Baray, J.-L., Bourassa, A.
1190 E., Cortesi, U., Degenstein, D. A., Froidevaux, L., Godin-Beekmann, S., Hoppel, K. W.,
1191 Johnson, B. J., Kyrölä, E., Leblanc, T., Lichtenberg, G., Marchand, M., McElroy, C. T.,

1192 Huijnen, V., Flemming, J., Chabrillat, S., Errera, Q., Christophe, Y., Blechschmidt, A.-M.,
1193 Richter, A., and Eskes, H.C-IFS-CB05-BASCOE: stratospheric chemistry in the Integrated
1194 Forecasting System of ECMWF, Geosci. Model Dev., 9, 3071-3091, 2016.
1195
1196 Hurrell, J. W.: Decadal trends in the North Atlantic Oscillation regional temperatures and
1197 precipitation, Science, 269, 676–679, 1995.
1198
1199 Hurtmans, D., P. Coheur, C.Wespes, L. Clarisse, O. Scharf, C. Clerbaux, J. Hadji-Lazaro, M.
1200 George, and S. Turquety: FORLI radiative transfer and retrieval code for IASI, Journal of
1201 Quantitative Spectroscopy and Radiative Transfer, 113, 1391-1408, 2012.
1202
1203 Jackman, C., E. Fleming, and F. Vitt: Influence of extremely large solar proton events in a
1204 changing stratosphere, J. Geophys. Res., 105, 11 659–11 670, 2000.
1205
1206 Jonsson, A. I., de Grandpré, J., Fomichev, V. I., McConnell, J. C., and Beagley, S. R.: Doubled
1207 CO2-induced cooling in the middle atmosphere: photochemical analysis of the ozone radiative
1208 feedback, J. Geophys. Res., 109, D24103, https://doi.org/10.1029/2004JD005093, 2004.
1209
1210 Kalnay, E., M. Kanamitsu, R. Kistler, W. Collins, D. Deaven, L. Gandin, M. Iredell, S. Saha, G.
1211 White, J. Woollen, Y. Zhu, M. Chelliah, W. Ebisuzaki, W. Higgins, J. Janowiak, K.C. Mo, C.
1212 Ropelewski, J. Wang, A. Leetmaa, R. Reynolds, R. Jenne, and D. Joseph, 1996: The
1213 NCEP/NCAR 40-Year Reanalysis Project. Bull. Amer. Meteor. Soc., 77, 437–472,
1214 https://doi.org/10.1175/1520-0477, 1996.
1215
1216 Keeble, J., Brown, H., Abraham, N. L., Harris, N. R. P., and Pyle, J. A.: On ozone trend
1217 detection: using coupled chemistry–climate simulations to investigate early signs of total column
1218 ozone recovery, Atmos. Chem. Phys., 18, 7625-7637, https://doi.org/10.5194/acp-18-7625-2018,
1219 2018.
1220
1221 Keppens, A., J.-C. Lambert, J. Granville, D. Hubert, T. Verhoelst, S. Compernolle, B. Latter, B.
1222 Kerridge, R. Siddans, A. Boynard, J. Hadji-Lazaro, C. Clerbaux, C. Wespes, D. R. Hurtmans, P.-
1223 F. Coheur, J. van Peet, R. van der A, K. Garane, M. E. Koukouli, D. S. Balis, A. Delcloo, R.
1224 Kivi, R. Stübi, S. Godin-Beekmann, M. Van Roozendael, C. Zehner: Quality assessment of the
1225 Ozone_cci Climate Research Data Package (release 2017): 2. Ground-based validation of nadir
1226 ozone profile data products, in preparation for this QOS special issue.
1227
1228 Kyrölä, E., Laine, M., Sofieva, V., Tamminen, J., Päivärinta, S.-M., Tukiainen, S., Zawodny, J.,
1229 and Thomason, L.: Combined SAGE II-GOMOS ozone profile data set for 1984–2011 and trend
1230 analysis of the vertical distribution of ozone, Atmos. Chem. Phys., 13, 10645–10658,
1231 https://doi.org/10.5194/acp-13-10645-2013, 2013.
1232
1233 Kodera, K. and Kuroda, Y.: Dynamical response to the solar cycle: Winter stratopause and lower
1234 stratosphere, J. Geophys. Res., 107, 4749, doi:310.1029/2002JD002224, 2002.
1235

Kuttippurath, J., F. Lefèvre, J.-P. Pommereau, H. K. Roscoe, F. Goutail, A. Pazmiño, J. D. Shanklin, Antarctic ozone loss in 1979–2010: First sign of ozone recovery. Atmos. Chem. Phys. 13, 1625–1635, doi:10.5194/acp-13-1625-2013, 2013.

Kuttippurath, J., and P.J. Nair: The signs of Antarctic ozone hole recovery 2017, Scientific Reports, **7**, 585, doi:10.1038/s41598-017-00722-7, 2017.

Labitzke, K. and van Loon, H.: The QBO effect on the solar signal in the global stratosphere in the winter of the Northern Hemisphere, J. Atmos. Solar-Terr. Phys., 62, 621–628, 2000.

Mäder, J. A., J. Staehelin, D. Brunner, W.A. Stahel, I. Wohltmann, and T. Peter: Statistical modelling of total ozone: Selection of appropriate explanatory variables, J. Geophys. Res., 112, D11108, doi:10.1029/2006JD007694, 2007.

Mäder, J. A., J. Staehelin, T. Peter, D. Brunner, H. E. Rieder, and W. A. Stahel: Evidence for the effectiveness of the Montreal Protocol to protect the ozone layer, Atmos. Chem. Phys., 10, 24, 12,161–12,171, doi:10.5194/acp-10-12161-2010, 2010.

Manatsa, D. and G. Mukwada: A connection from stratospheric ozone to El Niño-Southern Oscillation, Scientific Reports, 7, *5558*, DOI:10.1038/s41598-017-05111-8, 2017.

Manzini, E., Giorgetta, M. A., Esch, M., Kornblueh, L., and Roeckner, E.: The influence of sea surface temperatures on the northern winter stratosphere: Ensemble simulations with the MAECHAM5 model, J. Climate, 19, 3863–3881, 2006.

McCormack, J. P., D. E. Siskind, and L. L. Hood: Solar-QBO interaction and its impact on stratospheric ozone in a zonally averaged photochemical transport model of the middle atmosphere, *J. Geophys. Res.*, 112, D16109, doi:10.1029/2006JD008369, 2007.

McPeters, R. D., G.J. Labow, and J.A. Logan: Ozone climatological profiles for satellite retrieval algorithms, J. Geophys. Res.-Atmos., 112, D05308, doi:10.1029/2005JD006823, 2007.

Molina, M. J. and Rowland, F. S.: Stratospheric sink for chlorofluoromethanes: Chlorine atom-catalysed destruction of ozone, Nature, 249, 810–812, 1974.

Nair, P. J., Froidevaux, L., Kuttippurath, J., Zawodny, J. M., Russell, J. M., Steinbrecht, W., Claude, H., Leblanc, T., van Gijsel, J. A. E., Johnson, B., Swart, D. P. J., Thomas, A., Querel, R., Wang, R., and Anderson, J.: Subtropical and midlatitude ozone trends in the stratosphere: Implications for recovery, J. Geophys. Res.-Atmos., 120, 7247–7257, https://doi.org/10.1002/2014JD022371, 2015.

Newchurch, M. J., Yang, E.-S., Cunnold, D. M., Reinsel, G. C., Zawodny, J. M., and Russell III, J. M.: Evidence for slowdown in stratospheric ozone loss: First stage of ozone recovery, J. Geophys. Res., 108, 4507, doi:10.1029/2003JD003471, 2003.

1279 Newman, P. A., Nash, E. R., Kawa, S. R., Montzka, S. A., and Schauffler, S. M.: When will the
1280 Antarctic ozone hole recover?: Geophys. Res. Lett., 33, L12814, doi:10.1029/2005GL025232,
1281 2006.
1282
1283 Oman, L. D., Douglass, A. R., Ziemke, J. R., Rodriguez, J. M., Waugh, D. W., and Nielsen, J.
1284 E.: The ozone response to ENSO in Aura satellite measurements and a chemistry–climate
1285 simulation, J. Geophys. Res.-Atmos., 118, 965–976, 2013.
1286
1287 Pawson, S., Steinbrecht, W., Charlton-Perez, A J Fujiwara, M., Karpechko, A. Y.,
1288 Petropavlovskikh, I., Urban, J., and Weber, M.: Update on Global Ozone: Past, Present, and
1289 Future, in: Scientific Assessment of Ozone Depletion: 2014, World Meteorological
1290 Organization, Global Ozone Research and Monitoring Project – Report No. 55, chap. 2, World
1291 Meteorological Organization/UNEP, 2014.
1292
1293 Portmann, R. W., S. Solomon, R. R. Garcia, L. W. Thomason, L. R. Poole, M. P. McCormick,
1294 Role of aerosol variations in anthropogenic ozone depletion in the polar regions. J. Geophys.
1295 Res. 101, 22991–23006, doi:10.1029/96JD02608, 1996.
1296
1297 Knudsen, B. M. and Grooss, J.: Northern midlatitude stratospheric ozone dilution in spring
1298 modeled with simulated mixing, J. Geophys. Res., 105, 6885–6890, 2000.
1299
1300 Randel, W. J. and Cobb, J. B.: Coherent variations of monthly mean total ozone and lower
1301 stratospheric temperature, J. Geophys. Res.-Atmos., 99, 5433–5447, 1994.
1302
1303 Randel, W. J. and F. Wu: Isolation of the ozone QBO in SAGE II data by singular-value
1304 decomposition, J. Atmos. Sci., 53, 2546– 2559, 1996.
1305
1306 Randel, W. J., F. Wu, and R. Stolarski: Changes in column ozone correlated with the
1307 stratospheric EP flux, J. Meteorol. Soc. Jpn., 80, 849–862, 2002.
1308
1309 Randel, W. J., Garcia, R. R., Calvo, N., and Marsh, D.: ENSO influence on zonal mean
1310 temperature and ozone in the tropical lower stratosphere, Geophys. Res. Lett., 36, L15822,
1311 https://doi.org/10.1029/2009GL039343, 2009.
1312
1313 Randel, W. J., and A. M. Thompson: Interannual variability and trends in tropical ozone derived
1314 from SAGE II satellite data and SHADOZ ozonesondes, J. Geophys. Res., 116, D07303,
1315 doi:10.1029/2010JD015195, 2011.
1316
1317 Reinsel, G. C., Miller, A. J., Weatherhead, E. C., Flynn, L. E., Nagatani, R. M., Tiao, G. C., and
1318 Wuebbles, D. J.: Trend analysis of total ozone data for turnaround and dynamical contributions,
1319 J. Geophys. Res., 110, D16306, doi:10.1029/2004JD004662, 2005.
1320
1321 Revell, L. E., Stenke, A., Luo, B., Kremser, S., Rozanov, E., Sukhodolov, T., and Peter, T.:
1322 Impacts of Mt Pinatubo volcanic aerosol on the tropical stratosphere in chemistry–climate model

simulations using CCMI and CMIP6 stratospheric aerosol data, Atmos. Chem. Phys., 17, 13139-13150, 2017.

Rex, M., Salawitch, R. J., von der Gathen, P., Harris, N. R. P., Chipperfield, M. P., and Naujokat, B.: Arctic ozone loss and climate change, Geophys. Res. Lett., 32, L04116, doi:10.1029/2003GL018844, 2004.

Rieder, H. E., Frossard, L., Ribatet, M., Staehelin, J., Maeder, J. A., Di Rocco, S., Davison, A. C., Peter, T.,Weihs, P., and Holawe, F.: On the relationship between total ozone and atmospheric dynamics and chemistry at mid-latitudes – Part 2: The effects of the El Nino/Southern Oscillation, volcanic eruptions and contributions of atmospheric dynamics and chemistry to long-term total ozone changes, Atmos. Chem. Phys., 13, 165–179, 2013.

Rind, D., Perlwitz, J., and Lonergan, P.: AO/NAO response to climate change: 1. Respective influences of stratospheric and tropospheric climate changes, J. Geophys. Res., 110, D12107, doi: 10.1029/2004JD005103, 2005.

Rodgers, C. D.: Inverse Methods for Atmospheric Sounding: Theory and Practice, World Scientific, Series on Atmospheric, Oceanic and Planetary Physics, 2, Hackensack, N. J., 2000.

Salby, M., E. Titova, and L. Deschamps: Rebound of Antarctic ozone, *Geophys. Res. Lett.*, *38*, L09702, doi:10.1029/2011GL047266, 2011.

Schnadt, C. and Dameris, M.: Relationship between North Atlantic Oscillation changes and stratospheric ozone recovery in the Northern Hemisphere in a chemistry-climate model, J. Geophys. Res., 30, 1487, doi:10.1029/2003GL017006, 2003.

Shepherd, T. G., Plummer, D. A., Scinocca, J. F., Hegglin, M. I., Fioletov, V. E., Reader, M. C., Remsberg, E., von Clarmann, T., and Wang, H. J.: Reconciliation of halogen-induced ozone loss with the total-column ozone record, Nat. Geosci., 7, 443–449, https://doi.org/10.1038/ngeo2155, 2014.

Sioris, C. E., McLinden, C. A., Fioletov, V. E., Adams, C., Zawodny, J. M., Bourassa, A. E., Roth, C. Z., and Degenstein, D. A.: Trend and variability in ozone in the tropical lower stratosphere over 2.5 solar cycles observed by SAGE II and OSIRIS, Atmos. Chem. Phys., 14, 3479–3496, https://doi.org/10.5194/acp-14-3479-2014, 2014.

Sofieva, V. F., Kyrölä, E., Laine, M., Tamminen, J., Degenstein, D., Bourassa, A., Roth, C., Zawada, D., Weber, M., Rozanov, A., Rahpoe, N., Stiller, G., Laeng, A., von Clarmann, T., Walker, K. A., Sheese, P., Hubert, D., van Roozendael, M., Zehner, C., Damadeo, R., Zawodny, J., Kramarova, N., and Bhartia, P. K.: Merged SAGE II, Ozone_cci and OMPS ozone profile dataset and evaluation of ozone trends in the stratosphere, Atmos. Chem. Phys., 17, 12533–12552, https://doi.org/10.5194/acp-17-12533-2017, 2017.

1367 Solomon, S., Portman, R. W., Garcia, R. R., Thomason, L. W., Poole, L. R., and McCormack,
1368 M. P.: The role of aerosol variations in anthropogenic ozone depletion at northern midlatitudes,
1369 J. Geophys. Res., 101, 6713–6727, 1996.
1370
1371 Solomon, S.: Stratospheric ozone depletion: A review of concepts and history. Rev. Geophys.
1372 37, 275–316, doi:10.1029/1999RG900008, 1999.
1373
1374 Solomon, P., Barrett, J., Mooney, T., Connor, B., Parrish, A., and Siskind, D. E.: Rise and
1375 decline of active chlorine in the stratosphere, Geophys. Res. Lett., 33, L18807,
1376 https://doi.org/10.1029/2006GL027029, 2006.
1377
1378 Solomon, S., Ivy, D. J., Kinnison, D., Mills, M. J., Neely, R. R., and Schmidt, A.: Emergence of
1379 healing in the Antarctic ozone layer, Science, 353, 269–274,
1380 https://doi.org/10.1126/science.aae0061, 2016.
1381
1382 Soukharev, B. E. and L. L. Hood: Solar cycle variation of stratospheric ozone: Multiple
1383 regression analysis of long-term satellite data sets and comparisons with models, J. Geophys.
1384 Res., 111, D20314, doi:10.1029/2006JD007107, 2006.
1385
1386 Steinbrecht, W., H. Claude, U. Köhler, and K. P. Hoinka: Correlations between tropopause
1387 height and total ozone: Implications for long-term changes, *J. Geophys. Res.*, *103*, 19,183–
1388 19,192, doi:10.1029/98JD01929, 1998.
1389
1390 Steinbrecht, W., B. Hassler, H. Claude, P. Winkler, and R. S. Stolarski: Global distribution of
1391 total ozone and lower stratospheric temperature variations, Atmos. Chem. Phys., 3, 1421–1438,
1392 2003.
1393
1394 Steinbrecht, W., et al.: Interannual variation patterns of total ozone and lower stratospheric
1395 temperature in observations and model simulations, *Atmos. Chem. Phys.*, *6*, 349–374,
1396 doi:10.5194/acp-6-349-2006, 2006
1397
1398 Steinbrecht, W., Froidevaux, L., Fuller, R., Wang, R., Anderson, J., Roth, C., Bourassa, A.,
1399 Degenstein, D., Damadeo, R., Zawodny, J., Frith, S., McPeters, R., Bhartia, P., Wild, J., Long,
1400 C., Davis, S., Rosenlof, K., Sofieva, V., Walker, K., Rahpoe, N., Rozanov, A., Weber, M.,
1401 Laeng, A., von Clarmann, T., Stiller, G., Kramarova, N., Godin-Beekmann, S., Leblanc, T.,
1402 Querel, R., Swart, D., Boyd, I., Hocke, K., Kämpfer, N., Maillard Barras, E., Moreira, L.,
1403 Nedoluha, G., Vigouroux, C., Blumenstock, T., Schneider, M., García, O., Jones, N., Mahieu, E.,
1404 Smale, D., Kotkamp, M., Robinson, J., Petropavlovskikh, I., Harris, N., Hassler, B., Hubert, D.,
1405 and Tummon, F.: An update on ozone profile trends for the period 2000 to 2016, Atmos. Chem.
1406 Phys., 17, 10675–10690, doi:10.5194/acp-17-10675-2017, 2017.
1407
1408 Thomason, L. W., Ernest, N., Millán, L., Rieger, L., Bourassa, A., Vernier, J.-P., Manney, G.,
1409 Luo, B., Arfeuille, F., and Peter, T.: A global space-based stratospheric aerosol climatology:
1410 1979–2016, Earth Syst. Sci. Data, 10, 469-492, https://doi.org/10.5194/essd-10-469-2018, 2018.
1411

1412 Thompson, D. W. J. and J.M. Wallace: Annular modes in the extratropical circulation. Part I:
1413 month-to-month variability, J. Climate, 13, 1000–1016, 2000.
1414
1415 Thompson, D. W. J. and Solomon, S.: Interpretation of Recent Southern Hemisphere Climate
1416 Change, Science, 296, 895-899, 2002.
1417
1418 Tian, W., M.P. Chipperfield, L.J. Gray, and J.M. Zawodny: Quasi-biennial oscillation and tracer
1419 distributions in a coupled chemistry-climate model, J. Geophys. Res., 111, D20301,
1420 doi:10.1029/2005JD006871, 2006.
1421
1422 Tiao, G. C., G. C. Reinsel, D. Xu, J. H. Pedrick, X. Zhu, A. J. Miller, J. J. DeLuisi, C. L. Mateer,
1423 and D. J. Wuebbles, Effects of autocorrelation and temporal sampling schemes on estimates of
1424 trend and spatial correlation, J. Geophys Res., 95, 20,507-20,517, 1990.
1425
1426 Tweedy, O. V., Waugh, D. W., Randel, W. J., Abalos, M., Oman, L. D. and Kinnison, D. E.: The
1427 impact of boreal summer ENSO events on tropical lower stratospheric ozone, J.Geophys. Res.,
1428 Atmospheres, 123, 9843–9857, doi:10.1029/2018JD029020, 2018.
1429
1430 Valks, P., N. Hao, S. Gimeno Garcia, D. Loyola, M. Dameris, P. Jöckel, and A. Delcloo:
1431 Tropical tropospheric ozone column retrieval for GOME-2, Atmos. Meas. Tech., 7, 2513–2530,
1432 doi:10.5194/amt-7-2513-2014, 2014.
1433
1434 Vigouroux, C., Blumenstock, T., Coffey, M., Errera, Q., García, O., Jones, N. B., Hannigan, J.
1435 W., Hase, F., Liley, B., Mahieu, E., Mellqvist, J., Notholt, J., Palm, M., Persson, G., Schneider,
1436 M.,Servais, C., Smale, D., Thölix, L., and De Mazière, M.: Trends of ozone total columns and
1437 vertical distribution from FTIR observations at eight NDACC stations around the globe, Atmos.
1438 Chem. Phys., 15, 2915–2933, https://doi.org/10.5194/acp-15-2915-2015, 2015.
1439
1440 Weatherhead, E.C., G. C. Reinsel, G. C. Tiao, X.-L. Meng, D. Choi, W.-K. Cheang, T. Keller, J.
1441 DeLuisi, D. J. Wuebbles, J. B. Kerr, A. J. Miller, S. J. Oltmans and J. E. Frederick: Factors
1442 affecting the detection of trends: Statistical considerations and applications to environmental
1443 data, J. Geophys. Res. Atmos., 103, 17149–17161, 1998.
1444
1445 Weber, M., Coldewey-Egbers, M., Fioletov, V. E., Frith, S. M., Wild, J. D., Burrows, J. P.,
1446 Long, C. S., and Loyola, D.: Total ozone trends from 1979 to 2016 derived from five merged
1447 observational datasets – the emergence into ozone recovery, Atmos. Chem. Phys., 18, 2097–
1448 2117, https://doi.org/10.5194/acp-18-2097-2018, 2018.
1449
1450 Wespes, C., D. Hurtmans, L.K. Emmons, S. Safieddine, C. Clerbaux, D.P. Edwards, and P.-F.
1451 Coheur: Ozone variability in the troposphere and the stratosphere from the first six years of IASI
1452 observations (2008-2013), Atmos. Chem. Phys., 16, 5721-5743, 2016.
1453
1454 Wespes, C., D. Hurtmans, C. Clerbaux, and P.-F. Coheur: O_3 variability in the troposphere as
1455 observed by IASI over 2008–2016 — Contribution of atmospheric chemistry and dynamics, J.
1456 Geophys. Res. Atmos., 122, 2429–2451, doi:10.1002/2016JD025875, 2017.

Wespes, C., Hurtmans, D., Clerbaux, C., Boynard, A., and Coheur, P.-F.: Decrease in tropospheric O_3 levels in the Northern Hemisphere observed by IASI, Atmos. Chem. Phys., 18, 6867–6885, https://doi.org/10.5194/acp-18-6867-2018, 2018.

Witte, J. C., M.R. Schoeberl, A.R. Douglass, and A.M. Thompson: The Quasi-biennial Oscillation and annual variations in tropical ozone from SHADOZ and HALOE, Atmos. Chem. Phys., 8, 3929–3936, 2008.

World Meterological Organization (WMO): Scientific Assessment of Ozone Depletion: 2006, Global Ozone Research and Monitoring Project, Report No. 50, Geneva, Switzerland, 2007.

World Meterological Organization (WMO): Scientific Assessment of Ozone Depletion: 2010, Global Ozone Research and Monitoring Project, Report No. 52, Geneva, Switzerland, 2011.

World Meterological Organization (WMO): Scientific Assessment of Ozone Depletion: 2014, Global Ozone Research and Monitoring Project, Report No. 55, Geneva, Switzerland, 2014.

World Meterological Organization (WMO): Scientific Assessment of Ozone Depletion: 2018, Global Ozone Research and Monitoring Project, Report No. 58, Geneva, Switzerland, 2018.

Wohltmann, I., R. Lehmann, M. Rex, D. Brunner, and J. A. Maeder: A process-oriented regression model for column ozone, *J. Geophys. Res.*, *112*, D12304, doi:10.1029/2006JD007573, 2007.

Yang, E.-S., D. M. Cunnold, M. J. Newchurch, R. J. Salawitch, M. P. McCormick, J. M. Russell III, J. M. Zawodny, S. J. Oltmans: First stage of Antarctic ozone recovery. J. Geophys. Res. 113, D20308, doi:10.1029/2007JD009675, 2008.

Zerefos, C. S., Tourpali, K., Bojkov, R., Balis, D., Rognerund, B., and Isaksen, I.: Solar acticity – total ozone relationships: observations and model studies with heterogeneous chemistry, J. Geophys. Res., 102, 1561–1569, 1997.

Ziemke, J. R., A.R. Douglass, L.D. Oman, S.E. Strahan, and B.N. Duncan: Tropospheric ozone variability in the tropics from ENSO to MJO and shorter timescales, Atmos. Chem. Phys., 15, 8037–8049, 2015.